北京大学

本科生毕业论文

题目：离子阱系统中的量子阻尼

姓　　名：路尧

学　　号：1000011336

院　　系：物理学院

专　　业：物理专业

研究方向：量子信息

导　　师：金奇奂副教授

二零一四年六月

Content

List of Figures

Chapter 1

Introduction to Quantum Information

Quantum computer is regarded as the most powerful computing machine in the near future. It can handle such problems which are impossible to be solved by classical computer[1]. Meanwhile, security of communication[2] in quantum information is another aspect attracting researchers.

1.1 Basic Concepts in Quantum Information

In classical computer, the basic unit of computation is bit, as we know, "0" or "1". They are distinguished by the value of voltage, such as "0" represented by low voltage while "1" represented by high. However in quantum computer, we have qubit, which means "quantum bit". It is natural to choose different quantum states as qubit, noting $|0\rangle$ and $|1\rangle$. Fortunately, superposition of states is allowed in the quantum physics, so we can realize a state,

$$|\phi\rangle = \alpha|0\rangle + \beta|1\rangle \tag{1.1}$$

where α and β are arbitrary complex number and satisfy $|\alpha|^2 + |\beta|^2 = 1$. Such superposition of bits is unreachable in classical computer.

Another basic concept in quantum information is entangle state. Entangle is the quantum correlations between systems which can not define individual prop-

erties. Mathematically, an entangle state can not be written as the product of individual states. Such as Bell State and GHZ state, they are well-known entangle state. Entangle state is the essential component in quantum information, especially in quantum communication.

1.2 Requirements of Quantum Computation

To realize universal quantum computation protocols, there are several necessary requirements[3]:

1. state initialization of the qubits
2. long-lived coherences
3. universal set quantum gates
4. efficient qubit measurement
5. scalable to large number of qubits

There are several systems proposed to realize the quantum computation: superconductor circuits[4], quantum dots and dopants[5], ion trap system[6], optics[7], Nuclear Magnetic Resonance (NMR)[8], and so on. The ion trap system is what we now focus on.

1.3 Advantages of Ions Trap System

Comparing with other systems, the ion trap system has its own advantages:

1. Realize the initialization of ion state by optical pumping
2. Have long life time in the trap
3. Have the longest coherence time among known physical system
4. Detect with high efficiency over 99%
5. Control over internal and external degree easily

Chapter 2

Dynamics in Ion Trap System

2.1 Paul Trap

For a ion trap system, primary thing to realize is the trapping of ion. The electric field is first choice because of the charges with ion. According to the Maxwell Equations, a single ion cannot be trapped in a purely static electric field. To satisfy the equation in free space:

$$\nabla \cdot \vec{E} = 0 \ \ (or\ \Delta\Phi = 0) \tag{2.1}$$

it means that a electric field line enters into the region must go out the region. This requirement leads the result that a purely static electric field cannot trap a ion in all three dimensions. So other way is required.

One popular form of ion trap is Penning Trap[9], which combines static electric field and magnetic field together. Another form is called as Paul Trap[10], using spatially time-dependent electric field, typically oscillating at radio frequency (RF). In our setup, we use four-electrodes trap, one type of Paul Trap.

Seeing our setup in Figure 2.2, a radio frequency source is connected to the trap through amplification and helical resonator. An ion pump and a Ti sublimation pump are connected to the trap to make ultra-high vacuum environment lower than 10^{-11} torr.

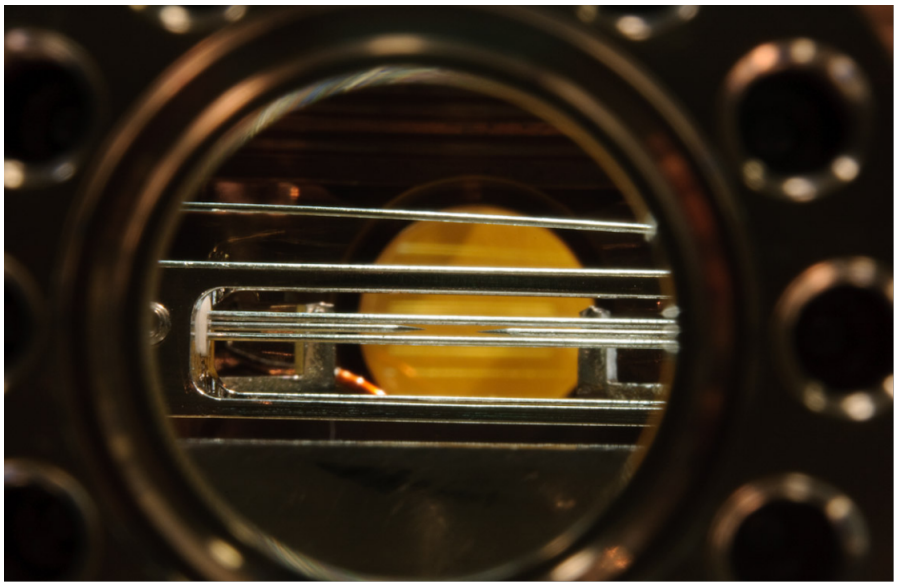

Figure 2.1: Four-electrodes Paul trap by courtesy of [11]

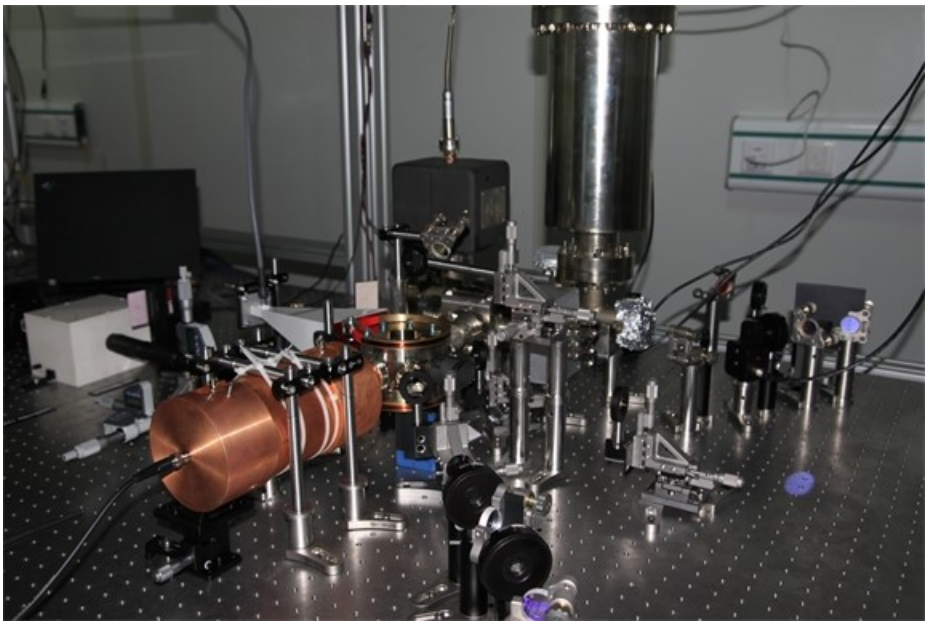

Figure 2.2: Ion trap used in CQI.

The potential of trap near axis is, generated by electrodes[12]:

$$\Phi(x,y,t) = \frac{U_0}{2}\cos(\Omega_T t)(1+\frac{x^2-y^2}{R^2}) \tag{2.2}$$

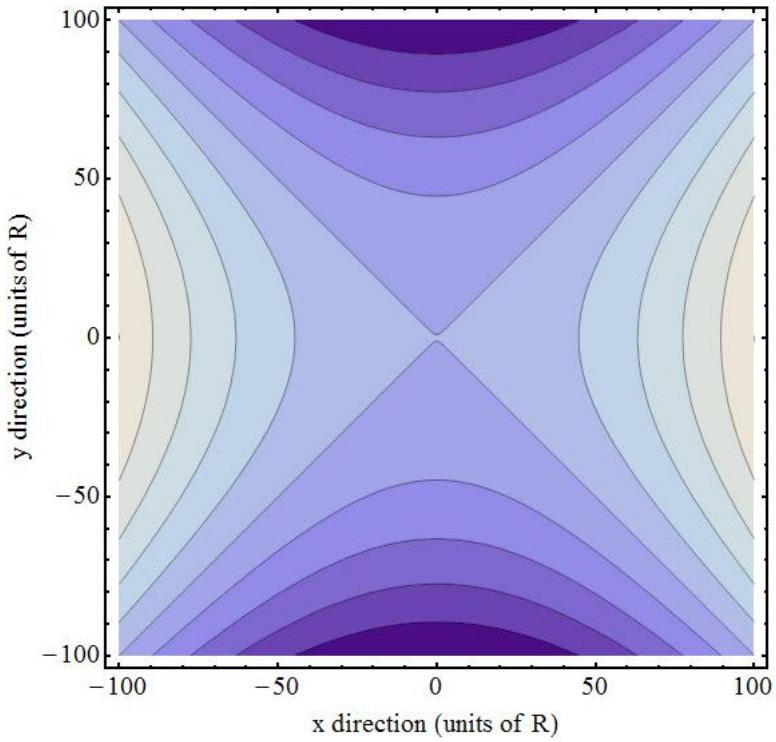

Figure 2.3: Hyperbolic electrodes. The resulting potential is shown for $t = 0$.

2.2 Pseudopotential: Harmonic Potential

Based on (2.2), we consider how ion moves in such a trap. Assuming an ion feels electric field $E(x,t)$ (for convenience considering x direction), the force applying on the ion is:

$$F = m\ddot{x} = eE(x,t) = eE_0(x)\cos(\Omega_T t) \tag{2.3}$$

if the electric field oscillates in cosine with frequency Ω_T. After integrating over time, we obtain:

$$x(t) = x_0 - \frac{eE_0(x)}{m\Omega_T^2}\cos(\Omega_T t) \tag{2.4}$$

assuming the initial position of ion is x_0. So the ion is oscillating near the x_0 with frequency Ω_T. We can expand the $E_0(x)$ for the position near the ion:

$$\begin{aligned} E_0(x) &= E_0(x_0) + \left.\frac{\partial E_0(x)}{\partial x}\right|_{x=x_0}(x - x_0) \\ &= E_0(x_0) + \frac{\partial E_0(x_0)}{\partial x_0}(\frac{eE_0(x)}{m\Omega_T^2}\cos(\Omega_T t)) \end{aligned} \tag{2.5}$$

Because of fast Ω_T, It is meaningful to consider force applying on the ion for time average. Obviously after time average, the part of $\cos(\Omega_T t)$ vanishes. The left part is:

$$\begin{aligned} \bar{F} &= -\frac{e^2}{2m\Omega_T^2}\frac{\partial E_0(x)}{\partial x}E_0 \\ &= -e\frac{\partial \psi_p}{\partial x} \end{aligned} \tag{2.6}$$

where we define pseudopotential[13] ψ_p as:

$$\psi_p = \frac{eE_0^2}{4m\Omega_T^2} \tag{2.7}$$

So in general we can derive that:

$$\bar{F} = -e\nabla\psi_p(x,y,z) \qquad \psi_p(x,y,z) = \frac{e(\vec{E}(x,y,z))^2}{4m\Omega_T^2} \tag{2.8}$$

Checking our trap, we have:

$$E(x,y,z) = -\nabla\Phi = -\frac{V_0}{R^2}(x\vec{e}_x - y\vec{e}_y) \tag{2.9}$$

The time average force applying on ion is:

$$\bar{F} = -\frac{e^2V_0^2}{2m\Omega_T^2R^4}(x\vec{e}_x - y\vec{e}_y) \tag{2.10}$$

Focusing on one dimension (take x direction for example), we have:

$$\bar{F}_x = m\ddot{x} = -\frac{e^2V_0^2}{2m\Omega_T^2R^4}x \tag{2.11}$$

It is easy to notice that the motion equation

$$\ddot{x} + \frac{e^2V_0^2}{2m^2\Omega_T^2R^4}x = 0 \tag{2.12}$$

is the equation of a harmonic oscillator with oscillating frequency

$$\omega_x = \frac{eV_0}{\sqrt{2}m\Omega_TR^2} \tag{2.13}$$

So does the y direction.

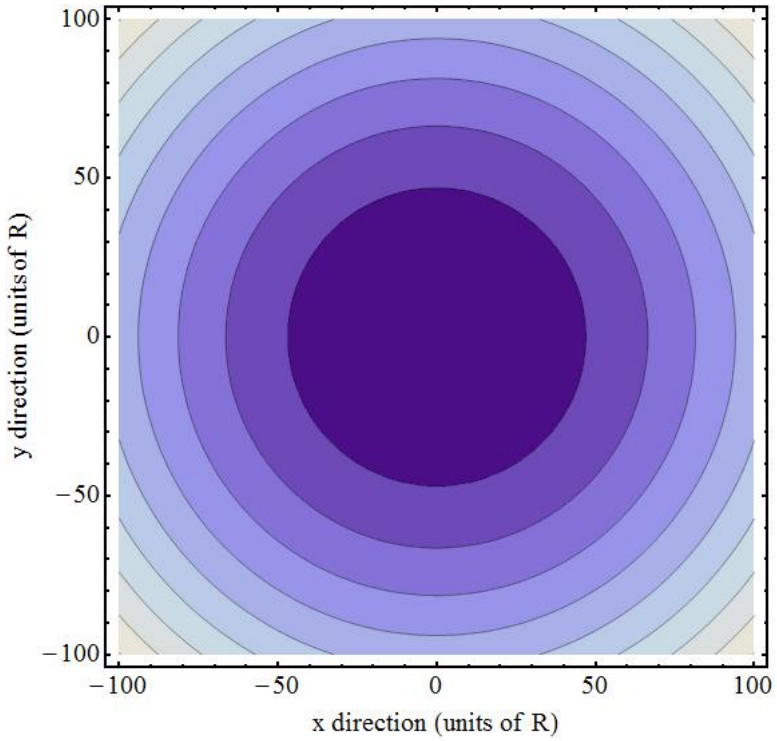

Figure 2.4: The pseudopotential derived from (2.8).

2.3 Mathieu Equation: Micromotion

Using pseudopotential approximation, we can roughly get the outline of the ion's motion in trap, but almost all the details are neglected. It is necessary to solve the motion equation more rigorous. Actually the precise solution to the dynamics of single trapped ion has been carefully studied [14].

Insert (2.2) into the motion equation of x direction:

$$\ddot{x} = -\frac{Z|e|}{m}\frac{\partial \Phi}{\partial x} \tag{2.14}$$

where m is the mass of ion and $Z|e|$ is the charge, we get the equation:

$$\ddot{x} + \frac{|Z|eV_0}{mR^2}x\cos(\Omega_T t) = 0 \tag{2.15}$$

Actually it is the form of Mathieu equation:

$$\frac{d^2x}{d\xi^2} + [a_x - 2q_x\cos(2\xi)]x = 0 \tag{2.16}$$

on substituting:

$$\xi = \frac{\Omega_T t}{2} \qquad a_x = 0 \qquad q_x = \frac{2|Z|eV_0}{m\Omega_T^2 R^2} \tag{2.17}$$

In the case $|a_x|, q_x^2 \ll 1$, the high orders of the solution to Mathieu equation can be neglected. The approximate solution is:

$$x(t) = x_0\cos(\omega_x t)[1 - \frac{q_x}{2}\cos(\Omega_T t)] \tag{2.18}$$

where x_0 is dependent on the boundary condition. ω_x in this case is:

$$\begin{aligned}\omega_x &= \frac{\Omega_T}{2}\sqrt{a_x + \frac{q_x^2}{2}} = \frac{q_x\Omega_T}{2\sqrt{2}} \\ &= \frac{|Z|eV_0}{\sqrt{2}m\Omega_T R^2}\end{aligned} \tag{2.19}$$

It is equal to (2.13) if we take $|Z|$ as 1. Obviously this part oscillating with frequency ω_x is corresponding to the approximation of pseudopotential. The second part is still a cosine oscillating part, with frequency Ω_T and a amplification modulation factor $q_x/2 \ll 1$. For $\Omega_T \gg \omega_x$, the ideal harmonic oscillation is overlapped with a smaller but faster oscillation, which is called as micromotion.

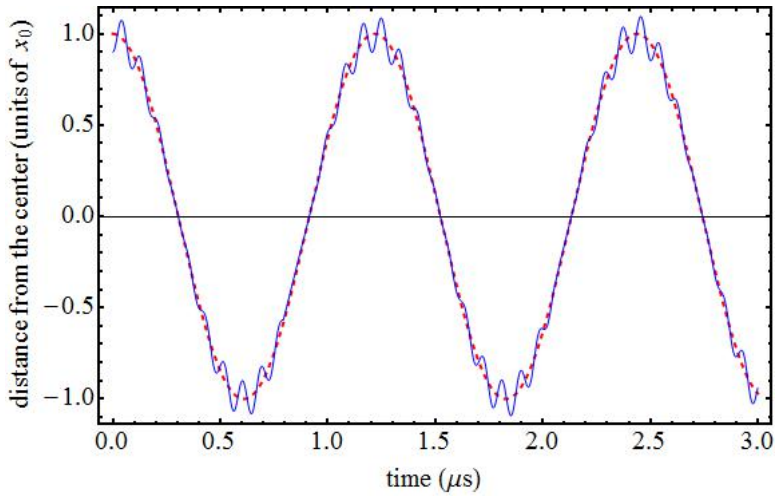

Figure 2.5: Ideal harmonic oscillation and the solution to Mathieu equation. The dashed line(red) is the harmonic oscillation, while solid(blue) line shows the result of micromotion.

2.4 Dynamics in Quantum Mechanics

In experiment we add two addition DC electrodes to confine the micromotion. So it is proper to regard the ion as a harmonic oscillator. Simply we can get the Hamiltonian of the motion of the ion in the trap:

$$\widehat{H}_m = (\widehat{a}^\dagger \widehat{a} + \frac{1}{2})\hbar\nu \tag{2.20}$$

Furthermore, for a harmonic oscillator, its eigenstates are the set of Fock State $|n\rangle$. We note they as the motion states of the ion with different energy phonon level $|n\rangle$.

Then, we consider a pair of qubit ($|\downarrow\rangle$ and $|\uparrow\rangle$ to distinguish from Fock state)

as a two level system. It's convenient to introduce Pauli Matrices:

$$\begin{aligned} \widehat{I} &= |\downarrow\rangle\langle\downarrow| + |\uparrow\rangle\langle\uparrow| \qquad \widehat{\sigma}_x = |\downarrow\rangle\langle\uparrow| + |\uparrow\rangle\langle\downarrow| \\ \widehat{\sigma}_y &= \mathrm{i}(|\downarrow\rangle\langle\uparrow| - |\uparrow\rangle\langle\downarrow|) \qquad \widehat{\sigma}_z = |1\rangle\langle\uparrow| - |\downarrow\rangle\langle\downarrow| \end{aligned} \tag{2.21}$$

So the Hamiltonian of the two level system is:

$$\begin{aligned} \widehat{H}_e &= \hbar\omega_\downarrow|\downarrow\rangle\langle\downarrow| + \hbar\omega_\uparrow|\uparrow\rangle\langle\uparrow| \\ &= \hbar\frac{\omega_0}{2}\widehat{\sigma}_z + \hbar\frac{\omega_\downarrow + \omega_\uparrow}{2}\widehat{I} \end{aligned} \tag{2.22}$$

where $\omega_0 = \omega_\uparrow - \omega_\downarrow$. It is no problem to ignore constant part, to rewrite $\widehat{H}_e$ as:

$$\widehat{H}_e = \hbar\frac{\omega_0}{2}\widehat{\sigma}_z \tag{2.23}$$

For $|\downarrow\rangle$ and $|\uparrow\rangle$, we note they as internal states.

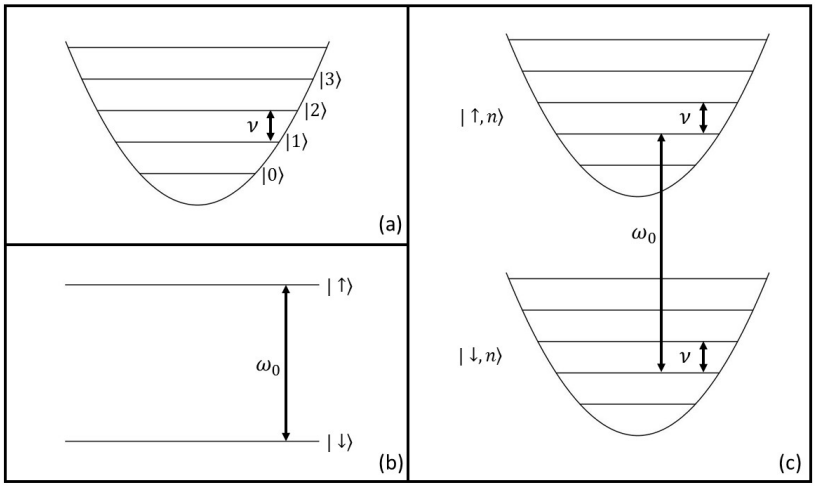

Figure 2.6: Motion state and internal state. (a) shows the motion state of an harmonic oscillator with frequency ν, the basis of state is Fock state $|n\rangle$. (b) shows the internal state of a simple two level system. (c) shows the coupling between the motion state and internal state.

Noticing that we have motion states $|n\rangle$ and internal states $|\downarrow\rangle$ and $|\uparrow\rangle$, we can easily couple them by laser. So the new space is the direct product of motion space

and internal space. The basics are noted as $|\uparrow, n\rangle$ and $|\downarrow, n\rangle$ (Shown in Figure 2.6).

If we note the Hamiltonian of interaction as $\widehat{H}_i$, the total Hamiltonian is:

$$\widehat{H} = \widehat{H}_m + \widehat{H}_e + \widehat{H}_i \tag{2.24}$$

What we care about is the coupling between motion states and internal states, therefore we transform into interaction picture with free Hamiltonian $\widehat{H}_0 = \widehat{H}_m + \widehat{H}_e$. Thus the interaction Hamiltonian is:

$$\widehat{H}_I = \widehat{U}_0^\dagger \widehat{H}_i \widehat{U}_0 \tag{2.25}$$

where $\widehat{U}_0 = \exp\left(-(i/\hbar)\widehat{H}_0 t\right)$. We will discuss this in detail in next chapter.

Chapter 3

Laser Setup, Ion initialization and Manipulation

3.1 Ytterbium and Laser Setup

It is common to question that why we choose Ytterbium (actually $^{171}Yb^{+}$) as trapped ion. In fact, several ions, such as $Ba^{+}, Be^{+}, Ca^{+}, Cd^{+}, Mg^{+}, Yb^{+}$, have been successfully manipulated in trap[13]. All ions mentioned above have a common feature. They are all hydrogen-like ions. This common point determines that they have similar level structure. In experiment, it is convenient to realize the transition through $^{2}S_{1/2}$and $^{2}P_{1/2}$. Meanwhile, other transitions among $^{2}S_{1/2}$, $^{2}P_{1/2}$, $^{2}D_{5/2}$and other energy level are also useful.

3.1.1 Laser Setup

The most efficient way to drive the transition is based on laser which energy of photon (or wavelength) satisfy the energy gap between levels of transition. For our $^{171}Yb^{+}$, several lasers we use are listed in the Figure 3.1 (in dashed black line):

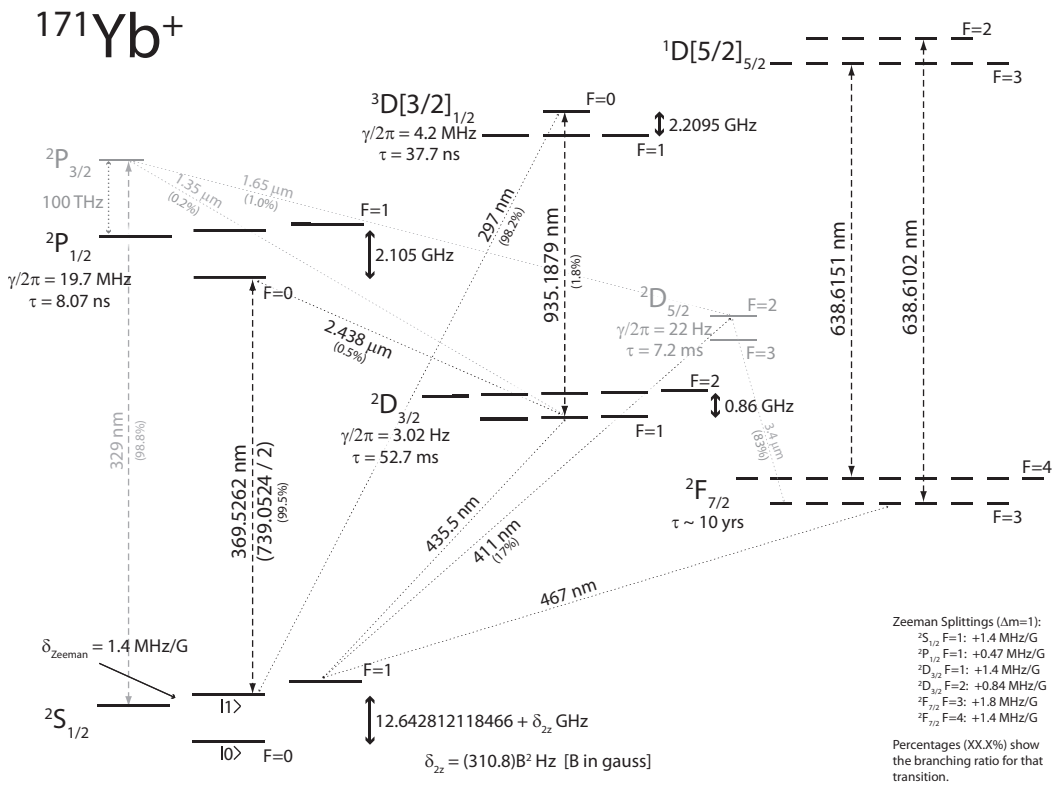

Figure 3.1: $^{171}Yb^{+}$fine and hyperfine structure (to scale), courtesy of [15]. The 369.53 nm laser is used for photoionization (with 398.9 nm laser), optical pumping, Doppler cooling and detection. 935 nm and 638 nm laser are used to take ion back from unexpected manifolds.

3.1.2 Hyperfine Qubit

Actually we put $^{171}Yb^{+}$in a fixed magnetic field, leading to Zeeman splitting or hyperfine structure of initial energy level. Here we choose two hyperfine levels as our qubit (as shown in Figure 3.1):

$$\begin{aligned} |\downarrow\rangle &= |^2S_{1/2}, F = 0, m_F = 0\rangle \\ |\uparrow\rangle &= |^2S_{1/2}, F = 1, m_F = 0\rangle \end{aligned} \tag{3.1}$$

3.2 Initialization of Ion

Initialization of ion is one of the key step to realize further manipulation. Here are several steps for initialization.

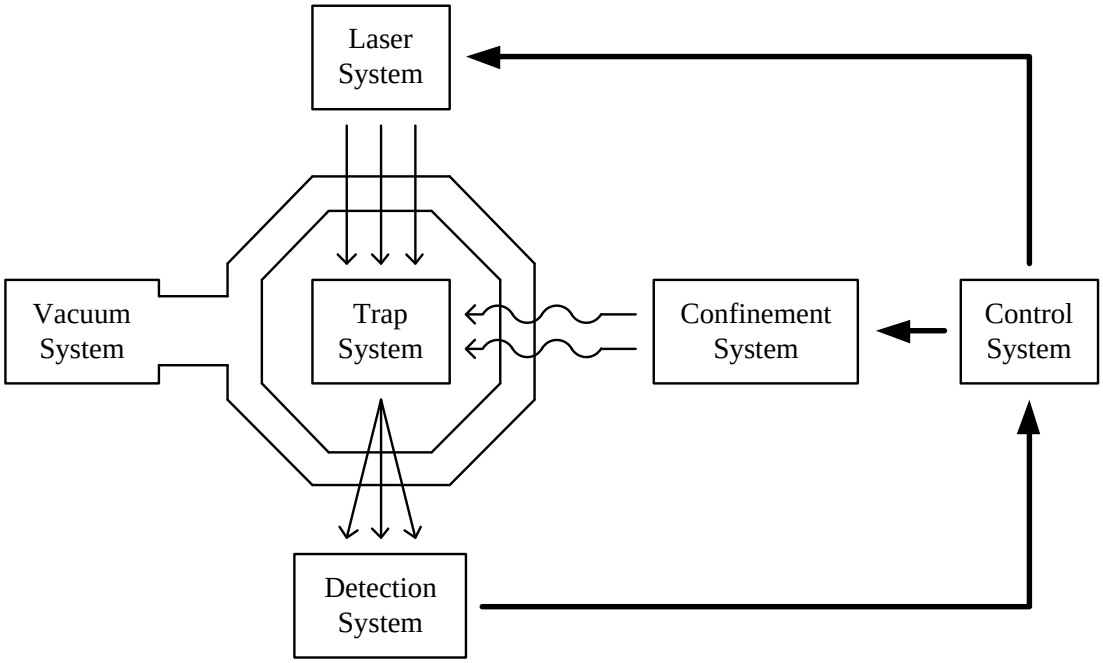

Figure 3.2: Divisions of our experimental system, courtesy of [16]

3.2.1 Photoionization

In fact $^{171}Yb^{+}$is loaded into the trap by the photoionization of neutral Yb. In the vacuum chamber (shown in Figure 2.2) the trap and ions guns are included. After applying current to the ion guns, atom beam is headed into the trap. With the help of two laser, the photoionization can be successfully achieved.

According to Figure 3.3, one beam is 398.9 nm, which is provided by Topica diode laser. Another is 369.53 nm which is the SHG laser from a 739.06 nm diode laser. Additionally, in order to avoid Doppler Effect, the direction of two laser beam should be approximately perpendicular to the atom beam.

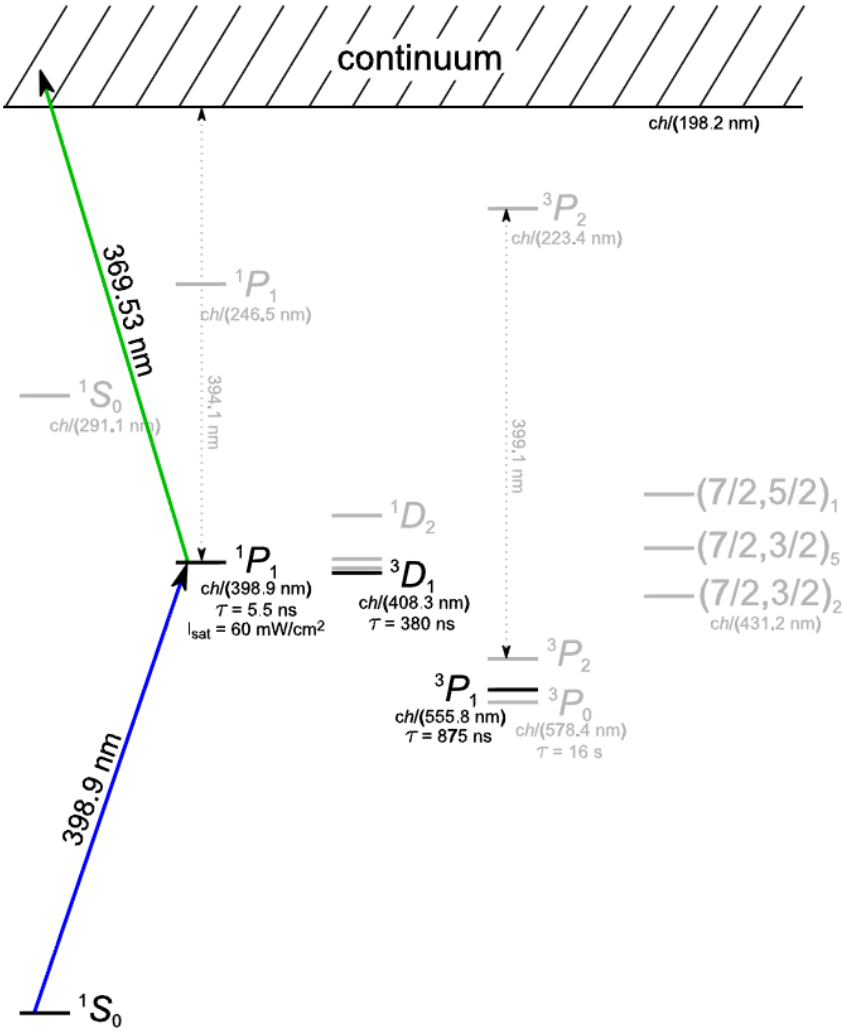

Figure 3.3: Partial level diagram of neutral Ytterbium atom (to scale). The process of photoionization is shown by courtesy of [13].

3.2.2 Doppler Cooling

After photoionization, we apply Doppler cooling[17] to the trapped $^{171}Yb^+$by 369.53 nm laser, which is slightly red detuned from $^2S_{1/2}|F=1\rangle \rightarrow {}^2P_{1/2}|F=0\rangle$.

For a incident light to be red detuned from resonance, because of Doppler Effect, the light frequency an atom feels is closer to resonance if an atom moves towards than it moves away. Considering an atom will absorb more photons when light frequency is closer to resonance, an atom will be slowed down in a certain

direction because of absorbing momentum of photons against atom.

However the spontaneous emission is still in random, so scattering in any other direction can heat the atom rather than cool it. The lowest temperature can be achieved is[18]

$$k_B T = \frac{\hbar\Gamma}{2} \tag{3.2}$$

where Γ is the rate of spontaneous emission.

In our case we use ${}^2S_{1/2}|F=1\rangle \rightarrow {}^2P_{1/2}|F=0\rangle$ as Doppler Cooling cycle. Because our laser can cause off-resonance coupling to ${}^2P_{1/2}|F=1\rangle$, the decay will cause ion trapped in $|\downarrow\rangle$, which limits the efficiency of cooling. So we add an Electro-Optic Modulator (EOM) driven at 7.37 GHz to couple $|\downarrow\rangle$ to prevent this. Furthermore, considering the opportunity of decay from ${}^2P_{1/2} \rightarrow D$, we still need laser 935 nm with an EOM driven at 3.07 GHz to bring state back to cooling cycle. Finally for the $S \rightarrow F$ caused by collision, we also need laser 638 nm.

3.2.3 Optical Pumping

It is important to initialize the state in $|\downarrow\rangle$ by optical pumping[19]. We use laser 369.53 nm with an EOM driven at 2.01 GHz, which couples the transition of ${}^2S_{1/2}|F=1\rangle \rightarrow {}^2P_{1/2}|F=1\rangle$. In this cycle all the state decay back to $|\downarrow\rangle$ will be trapped and can not come back to the cycle. After finite cycles (in our experiment about 1 μs), most of the state will be in $|\downarrow\rangle$

3.2.4 Detection

To do the state detection, we still use ${}^2S_{1/2}|F=1\rangle \rightarrow {}^2P_{1/2}|F=0\rangle$ transition. If the ion is at $|\uparrow\rangle$, there will be enough scattering photons. On the contrary, if the ion is at $|\downarrow\rangle$, there will be less photons.

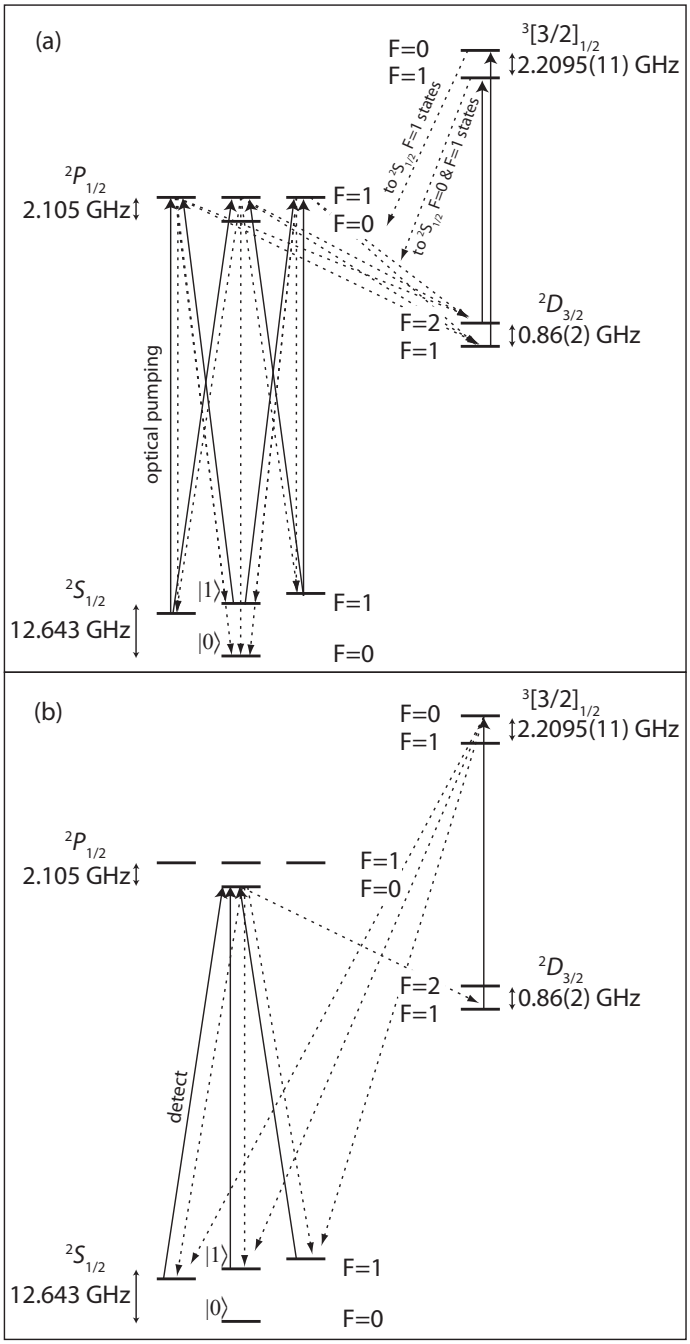

Figure 3.4: The process of initialization by courtesy of [20]. (a) refers to optical pumping. 369.53 nm laser with EOM driven at 2.105 GHz is used to coupling of $^2P_{1/2}|F=1\rangle$ levels. (b) refers to the detection of the qubit state.

3.3 Raman Transition

3.3.1 General Theory of Two Level Transition

As we mentioned in last chapter, the total Hamiltonian applying on the ion can be describe as (2.24). In recent researches of interaction, what we focus on can be simplified as the transition in a two level system. For running wave light field case, coupling Hamiltonian can be described as[14]

$$\widehat{H}_i = \frac{\hbar\Omega}{2}(\widehat{\sigma}_+ + \widehat{\sigma}_-) \times [e^{i(k\widehat{x}-\omega t+\phi)} + e^{-i(k\widehat{x}-\omega t+\phi)}] \tag{3.3}$$

Transforming it into interaction picture in (2.25) way, the interaction Hamiltonian is

$$\begin{aligned}\widehat{H}_I &= \widehat{U}_0^\dagger \widehat{H}_i \widehat{U}_0 \\ &= \frac{\hbar\Omega}{2} e^{(i/\hbar)\widehat{H}_e t}(\widehat{\sigma}_+ + \widehat{\sigma}_-)e^{(-i/\hbar)\widehat{H}_e t} \\ &\times e^{(i/\hbar)\widehat{H}_m t}[e^{i(k\widehat{x}-\omega t+\phi)} + e^{-i(k\widehat{x}-\omega t+\phi)}]e^{(-i/\hbar)\widehat{H}_m t}\end{aligned} \tag{3.4}$$

For part $e^{(i/\hbar)\widehat{H}_m t}\widehat{x}e^{(-i/\hbar)\widehat{H}_m t}$, it is the transformation from Schrodinger picture to Heisenberg picture, which means

$$e^{(i/\hbar)\widehat{H}_m t}\widehat{x}e^{(-i/\hbar)\widehat{H}_m t} = \widehat{x}_H(t) \tag{3.5}$$

According to the derivation in reference [14], we have

$$k\widehat{x}_H(t) \approx \eta(\widehat{a}e^{-i\nu t} + \widehat{a}^\dagger e^{i\nu t}) \tag{3.6}$$

This equation is only established when $\eta \ll 1, (|a_x, q_x^2| \ll 1)$. The parameter η is called as Lamb-Dicke parameter, which is equal to $\eta = kx_0 = k\sqrt{\hbar/(2m\nu)}$. Obvi-

ously x_0 is the extension of the wave package of ground motion state. Lamb-Dicke parameter is essential parameter in ion trap system. We confine our experiment in Lamb-Dicke region for $\eta \ll 1$ (in experiment $\eta \approx 0.098$), where harmonic oscillator can be a ideal approximation.

Now inserting (3.6) into (3.4), in reference [14] the final result is

$$\widehat{H}_I = \frac{\hbar\Omega_0}{2}\widehat{\sigma}_+ \exp\left[i\eta(\widehat{a}e^{-i\nu t} + \widehat{a}^\dagger e^{i\nu t})\right]e^{i(\phi-\delta t)} \tag{3.7}$$

where $\Omega_0 = \Omega/(1 + q_x/2)$ is the approximation of solution of low orders in Lamb-Dicke region. And $\delta = \omega - \omega_0$ is the detuning between light frequency and energy gap of two level system. Depending on the δ, the interaction Hamiltonian will couple certain internal state ($|\uparrow\rangle$ or $|\downarrow\rangle$) and motion state ($|n\rangle$). With $\delta = \pm s\nu$, the interaction Hamiltonian can drive different sideband transition between $|\downarrow, n\rangle$ and $|\uparrow, n \pm s\rangle$. The coupling strength, or often called as Rabi frequency, is calculated as

$$\begin{aligned}\Omega_{n,n+s} = \Omega_{n+s,n} &= \Omega_0|\langle n+s|e^{i\eta(\widehat{a}+\widehat{a}^\dagger)}|n\rangle| \\ &= \Omega_0 e^{-\eta^2/2}\eta^{|s|}\sqrt{\frac{n_<!}{n_>!}}L_{n_<}^{|s|}(\eta^2)\end{aligned} \tag{3.8}$$

where $n_<(n_>)$ is the smaller(bigger) one between n and $n+s$. $L(\eta^2)$ refers to Laguerre function. However, in Lamb-Dicke region, the higher orders of sideband transition is too small to neglect. What we are interested in are only 0th and 1st orders, called as carrier transition (for $\delta = 0$), red sideband transition (for $\delta = -\nu$) and blue sideband transition (for $\delta = \nu$). The Hamiltonian can be expressed as:

1. Carrier transition between $|\downarrow, n\rangle$ and $|\uparrow, n\rangle$

$$\widehat{H}_{car} = \frac{\hbar\Omega_0}{2}(\widehat{\sigma}_+ e^{i\phi} + \widehat{\sigma}_- e^{-i\phi}) \tag{3.9}$$

2. Red sideband transition between $|\downarrow, n\rangle$ and $|\uparrow, n-1\rangle$

$$\widehat{H}_{rsb} = \frac{\hbar\eta\Omega_0}{2}(\widehat{a}\widehat{\sigma}_+ e^{i\phi} + \widehat{a}^\dagger\widehat{\sigma}_- e^{-i\phi}) \tag{3.10}$$

3. Blue sideband transition between $|\downarrow, n\rangle$ and $|\uparrow, n+1\rangle$

$$\widehat{H}_{bsb} = \frac{\hbar\eta\Omega_0}{2}(\widehat{a}^\dagger\widehat{\sigma}_+ e^{i\phi} + \widehat{a}\widehat{\sigma}_- e^{-i\phi}) \tag{3.11}$$

Actually when η is small enough the coupling strength or Rabi frequency can be approximated as

$$\begin{aligned} \Omega_{n,n} &= \Omega_0 \\ \Omega_{n,n-1} &= \eta\Omega_0\sqrt{n} \\ \Omega_{n,n+1} &= \eta\Omega_0\sqrt{n+1} \end{aligned} \tag{3.12}$$

in turn correspond to carrier, red sideband and blue sideband transition. Furthermore, to measure the Rabi frequency of $\Omega_{0,1}$ and $\Omega_{0,0}$, we can estimate the value of Lamb-Dicke parameter with $\eta = \Omega_{0,1}/\Omega_{0,0}$.

For a initial state $|\Phi(0)\rangle = \sum_{n=0}^{\infty} c_n|\downarrow, n\rangle$, if we drive with blue sideband transition, the possibility that ion locate in $|\uparrow\rangle$ over time is:

$$P_{\uparrow,bsb}(t) = \sum_{n=0}^{\infty} \frac{1}{2} p_n[1 - \cos(\Omega_{n,n+1}t)] \tag{3.13}$$

where $p_n = |c_n|^2$ is the initial phonon population in $|\downarrow, n\rangle$ phonon level. For convenience we note $|\downarrow n\rangle$ as $|n\rangle$ because what we focus on is the phonon distribution in $|\downarrow\rangle$. At the same way, for red sideband transition, the possibility is:

$$P_{\uparrow,rsb}(t) = \sum_{n=1}^{\infty} \frac{1}{2} p_n[1 - \cos(\Omega_{n,n-1}t)] \tag{3.14}$$

The index begins from $n = 1$ because the population in $|\downarrow, 0\rangle$ can not go anywhere.

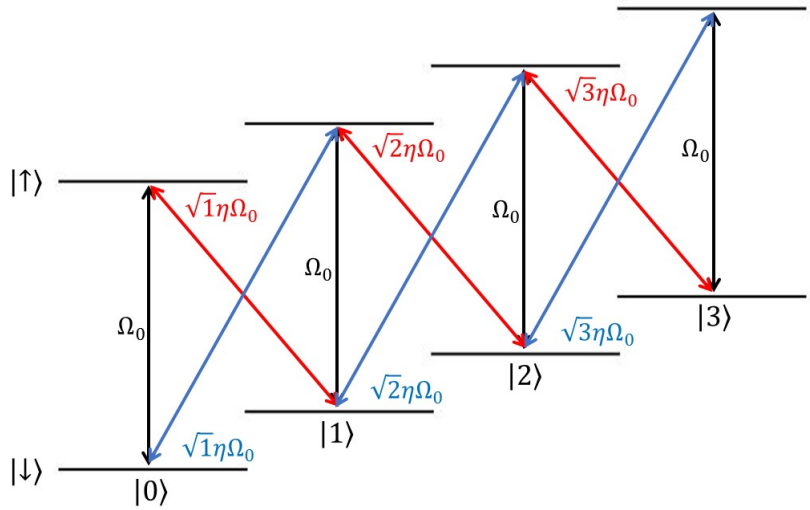

Figure 3.5: The process of different sideband transitions. Black lines refer to carrier transition with nearly same speed. Blue lines refer to blue sideband transition with ratio $\sqrt{n+1}$. Red lines refer to red sideband transition with ratio $\sqrt{n}$.

We find that the phonon distributions oscillate between $|\downarrow, n\rangle$ and $|\uparrow, n \pm s\rangle$ at Rabi frequency $\Omega_{n,n\pm s}$. This is called as Rabi oscillation. We define π pulse $(t - t_0 = \pi/\Omega_{n,n\pm s})$ which will exchange the distribution of $|\downarrow, n\rangle$ and $|\uparrow, n \pm s\rangle$, while $\pi/2$ pulse $(t - t_0 = \pi/2\Omega_{n,n\pm s})$ will exchange the distribution at half.

3.3.2 Stimulated Raman Transition

In experiment we use two photons stimulated Raman transition[18] as an effective way to drive the coupling between internal state and motion state. Considering three level system($|\downarrow\rangle, |\uparrow\rangle, |e\rangle$) with allowed transitions $|\downarrow\rangle \rightarrow |e\rangle$ and $|\uparrow\rangle \rightarrow |e\rangle$, we use two laser beams:

$$\begin{aligned} \vec{E}_1 &= \vec{\epsilon}_1 e^{i(\vec{k}_1\vec{x} - \omega_1 t)} + c.c \\ \vec{E}_2 &= \vec{\epsilon}_2 e^{i(\vec{k}_2\vec{x} - \omega_2 t)} + c.c \end{aligned} \tag{3.15}$$

which are detuned by Δ_e from $|e\rangle$.

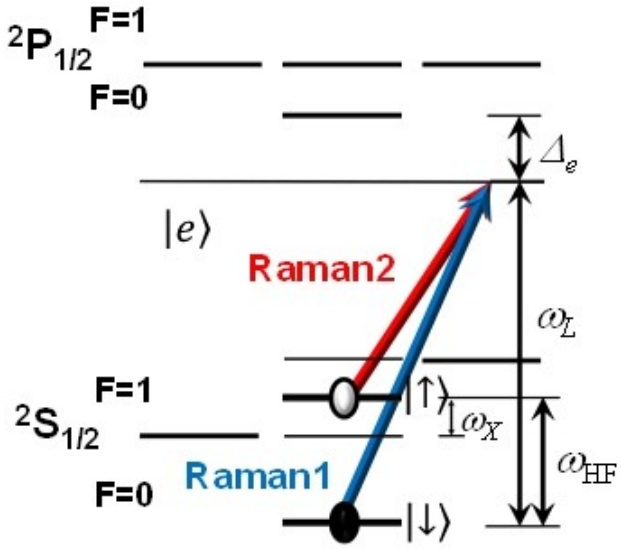

Figure 3.6: Stimulated Raman transition of $^{171}Yb^+$.

Noting $\Delta k = \vec{k}_2 - \vec{k}_1$ and $\Delta\omega = \omega_2 - \omega_2 = \omega_0 + \delta\omega$, courtesy of [14], the effective Hamiltonian applying on the ion is:

$$\widehat{H}_{eff} = -\frac{\hbar\Omega(\widehat{\sigma}_+ + \widehat{\sigma}_-)}{2}(e^{i(\Delta k\widehat{x} - \Delta\omega t + \phi)} + e^{-i(\Delta k\widehat{x} - \Delta\omega t + \phi)}) \tag{3.16}$$

where Ω is the Rabi frequency which represents the coupling strength between $|\downarrow\rangle, |\uparrow\rangle$. Noticing that (3.16) is in the same form of (3.3), so in the similar way, stimulated Raman transition can drive sideband transition to couple motion state and internal state, where the $\delta = \Delta - \omega_0$ determines the type of the sideband transition.

With the realization of sideband transition by stimulated Raman transition, resolved sideband cooling (RSB)[21] is an important sub-product. In fact, the phonon distribution of motional state reflects the motion of the ion, which is related to the temperature of the ion. Actually the relationship between temperature of the ion and phonon distribution is: $k_B T = \langle n\rangle\hbar\nu$, where $\langle n\rangle = \sum_n np_n$ is defined as average phonon number. In last section, we introduce Doppler cooling to cool the ion. However, because of Doppler cooling limit, the average phonon number after Doppler

cooling is still around 10. It is not cool enough to realize precise state preparation. Thus based on sideband transition, we try to realize sideband cooling.

The principle for resolved sideband cooling is very simple. For a initial state $|\downarrow, n\rangle (n > 0)$, after series sequences of ideal pure carrier transition and red sideband transition, it will finally go back, or cooling to $|\downarrow, 0\rangle$.

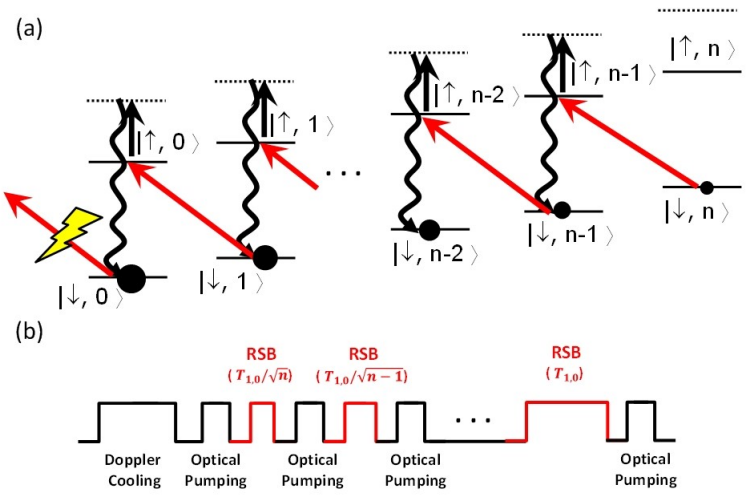

Figure 3.7: Sequence of resolved sideband cooling.

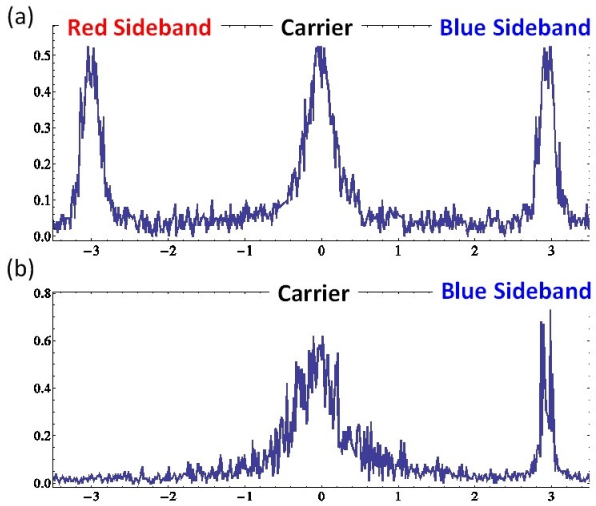

Figure 3.8: Result of resolved sideband cooling. (a) shows the result before resolved sideband cooling. there are some distributions in high n phonon state, so red sideband is allowed. (b) shows that, after sideband cooling, red sideband is forbidden because all phonon is trapped in $|0\rangle$ and no level to go.

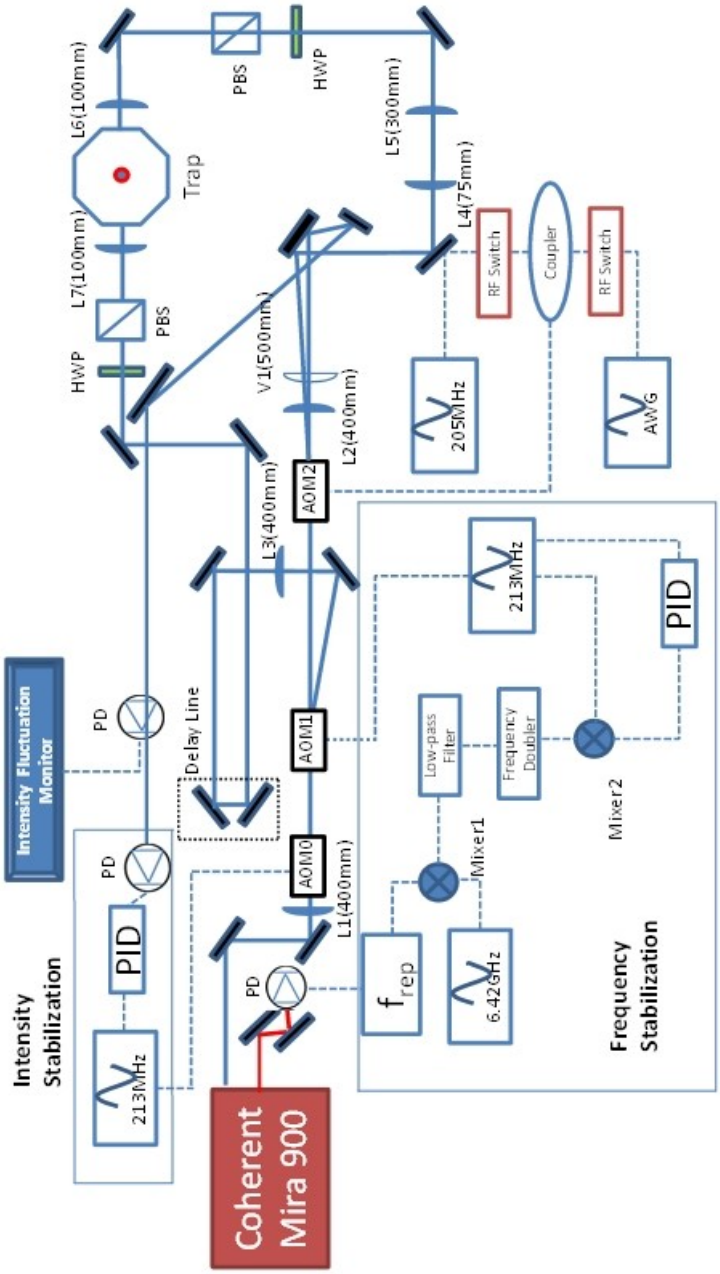

Figure 3.9: The path of our Raman laser system. Acousto-optical Modulators (AOM) are used to add frequency different detuning to Raman 1 laser and Raman 2 laser in order to drive different sideband transition. Two Raman beams propagate in opposite direction. Frequency stabilization is aimed to stable the frequency of laser as far as possible.

Chapter 4

Quantum Damping: Model for Heating Effect

When it comes to quantum computation, one of the most important factor we concern about is decoherence caused by environment, or interaction with environment, because the decoherence time determines the effective time to realize quantum computation. In ion trap system, the decoherence of motional state has been studied for a long time. In details the decoherence of motional state refers to the distribution in certain phonon level will tend to flux to nearby levels. It turns out to be a spread of distribution in motional state:

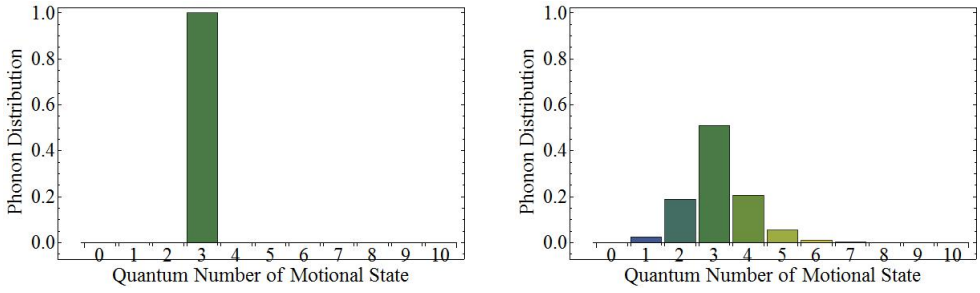

(a) Initial state $|n = 3\rangle$

(b) Simulation result after 1000 μs without other Hamiltonian

Figure 4.1: Take initial $|n = 3\rangle$ for example. In the simulation, the parameters are set up to experimental case. After only 1000 μs, the distribution spread beyond our expectation.

Meanwhile, the spread of phonon distribution accompanies with the increasing of average phonon number. In this reason, this decoherence is regard as heating

effect. The speed of average phonon increasing is called as heating rate.

In recent researches, the factors inducing heating effect have been studied for a long time. The most convincing reason is the electronic noise in the trap[22]. Thermal electronic noise and fluctuating patch-potential noise have been studied for heating dynamics. Several experimental parameters have also been considered. Geometry of the trap[22], distance between ion and electrodes[22, 23], the frequency of trap[22, 23] are part of factors affecting heating effect.

Actually the heating effect is regarded as a harmonic oscillator connecting to a thermal amplitude reservoir [24]. It is called as quantum damping in quantum optics. Based on *Quantum Optics* written by Scully[25], we derive and measure the heating rate in our ion trap system.

4.1 Theory of Quantum Damping

Considering a system interacting with a reservoir, we can writing the Master equation as:

$$i\hbar\dot{\rho}_{SR} = [\widehat{V}(t), \rho_{SR}] \tag{4.1}$$

where S represents "system" while R represents reservoir, $\widehat{V}(t)$ is the Hamiltonian of interaction between system and reservoir. We can formally integrate the equation:

$$\rho_{SR}(t) = \rho_{SR}(t_i) - \frac{i}{\hbar}\int_{t_i}^{t}[\widehat{V}(t'), \rho_{SR}(t')]dt' \tag{4.2}$$

where t_i is the beginning time of interacting. After inserting (4.2) into (4.1), we find the equation

$$i\hbar\dot{\rho}_{SR} = -\frac{i}{\hbar}[\widehat{V}(t), \rho_{SR}(t_i)] - \frac{1}{\hbar^2}\int_{t_i}^{t}[\widehat{V}(t), [\widehat{V}(t'), \rho_{SR}(t')]]dt' \tag{4.3}$$

If the system and the reservoir are independent, the density matrix can be easily factored into a direct product $\rho_{SR}(t) = \rho_S(t)\otimes\rho_R(t_i)$, where we assume the reservoir

at equilibrium. Due to weak coupling between the system and reservoir, we rewrite density matrix as

$$\rho_{SR}(t) = \rho_S(t) \otimes \rho_R(t_i) + \rho_c(t) \tag{4.4}$$

However, what we focus on is the density matrix of system, so we have the reduce matrix $\rho_S = Tr_R[\rho_{SR}]$. The master equation of the system can be derived:

$$\begin{aligned} \dot{\rho}_S &= -\frac{i}{\hbar} Tr_R[\widehat{V}(t), \rho_S(t_i) \otimes \rho_R(t_i)] \\ &- \frac{1}{\hbar^2} Tr_R \int_{t_i}^{t} [\widehat{V}(t), [\widehat{V}(t'), \rho_S(t') \otimes \rho_R(t_i)]] dt' \end{aligned} \tag{4.5}$$

For further discussion, the second term of the equation tells us that the reduced density matrix also depends on the past history of the evolution from t_i to t', described as Markov process. Fortunately, we assume that the damping process destroys all the memories of past, so we can treat it as non-Markovian. The evolution can be described as:

$$\begin{aligned} \dot{\rho}_S &= -\frac{i}{\hbar} Tr_R[\widehat{V}(t), \rho_S(t_i) \otimes \rho_R(t_i)] \\ &- \frac{1}{\hbar^2} Tr_R \int_{t_i}^{t} [\widehat{V}(t), [\widehat{V}(t'), \rho_S(t) \otimes \rho_R(t_i)]] dt' \end{aligned} \tag{4.6}$$

For a certain case, we consider reservoir of harmonic oscillator which can be described by operators $\widehat{b}_k^\dagger$ and $\widehat{b}_k$ coupling to another harmonic oscillator described by $\widehat{a}^\dagger$ and $\widehat{a}$. So the Hamiltonian of interaction can be written as:

$$\widehat{V}(t) = \hbar \sum_k (g_k \widehat{b}_k^\dagger \widehat{a} e^{-i(\omega - \nu_k)} + g_k^* \widehat{b}_k \widehat{a}^\dagger e^{i(\omega - \nu_k)}) \tag{4.7}$$

In this case, when the time scale we measure is larger than the period of harmonic oscillator, it is fine to consider the process as non-Markov process[26]. So we can

substitute the interaction Hamiltonian into evolution equation (4.6) and obtain:

$$\begin{aligned}\dot{\rho}_S = &-i\sum_k g_k\langle\widehat{b}_k^\dagger\rangle[\widehat{a},\rho_S(t_i)]e^{-i(\omega-\nu_k)t}\\ &-\int_{t_i}^{t}dt'\sum_{k,k'}g_kg_{k'}2[[\widehat{a}\widehat{a}\rho_S(t')-2\widehat{a}\rho_S(t')\widehat{a}+\rho_S(t')\widehat{a}\widehat{a}]\times e^{-i(\omega-\nu_k)t-i(\omega-\nu_{k'})t'}\langle\widehat{b}_k^\dagger b_{k'}^\dagger\rangle\\ &+[\widehat{a}\widehat{a}^\dagger\rho_S(t')-\widehat{a}^\dagger\rho_S(t')\widehat{a}]\times e^{-i(\omega-\nu_k)t+i(\omega-\nu_{k'})t'}\langle\widehat{b}_k^\dagger b_{k'}\rangle\\ &+[\widehat{a}^\dagger\widehat{a}\rho_S(t')-\widehat{a}\rho_S(t')\widehat{a}^\dagger]\times e^{i(\omega-\nu_k)t-i(\omega-\nu_{k'})t'}\langle\widehat{b}_k b_{k'}^\dagger\rangle]+H.c.\end{aligned} \tag{4.8}$$

If the reservoir is also in thermal equilibrium, the matrix ρ_R can be represented as:

$$\rho_R=\prod_k[1-\exp(-\frac{\hbar\nu_k}{k_BT})]\exp(-\frac{\hbar\nu_k\widehat{b}_k^\dagger\widehat{b}_k}{k_BT}) \tag{4.9}$$

So we can easily get:

$$\begin{aligned}\langle\widehat{b}_k\rangle&=\langle\widehat{b}_k^\dagger\rangle=0\\ \langle\widehat{b}_k^\dagger\widehat{b}_{k'}\rangle&=\bar{n}_k\delta_{kk'}\\ \langle\widehat{b}_k\widehat{b}_{k'}^\dagger\rangle&=(\bar{n}_k+1)\delta_{kk'}\\ \langle\widehat{b}_k\widehat{b}_{k'}\rangle&=\langle\widehat{b}_k^\dagger\widehat{b}_{k'}^\dagger\rangle=0\end{aligned} \tag{4.10}$$

where $\bar{n}_k$ is the average phonon number

$$\bar{n}_k=\frac{1}{\exp(\frac{\hbar\nu_k}{k_BT})-1} \tag{4.11}$$

Inserting (4.10) into (4.8), we obtain:

$$\begin{aligned}\dot{\rho}_S = & \\ -\int_{t_i}^{t} dt' \sum_k |g_k|^2 [[\widehat{a}\widehat{a}^\dagger \rho_S(t') - \widehat{a}^\dagger \rho_S(t')\widehat{a}]\bar{n}_k e^{-i(\omega-\nu_k)(t-t')} & \\ + [\widehat{a}^\dagger \widehat{a}\rho_S(t') - \widehat{a}\rho_S(t')\widehat{a}^\dagger](\bar{n_k}+1)e^{i(\omega-\nu_k)(t-t')}] + H.c. &\end{aligned} \tag{4.12}$$

To sum over the k, we can replace sum by integral through all k space.

$$\sum_k \longrightarrow 2\frac{V}{(2\pi)^3}\int_0^{2\pi} d\phi \int_0^{\pi} d\theta \sin\theta \int_0^{\infty} dk\ k^2 \tag{4.13}$$

So the final evolution equation is

$$\begin{aligned}\dot{\rho_S}(t) = -\bar{n}_{th}\frac{\Gamma}{2}[\widehat{a}\widehat{a}^\dagger \rho_S(t) - 2\widehat{a}^\dagger \rho_S(t)\widehat{a} + \rho_S(t)\widehat{a}\widehat{a}^\dagger] & \\ -(\bar{n}_{th}+1)\frac{\Gamma}{2}[\widehat{a}^\dagger \widehat{a}\rho_S(t) - 2\widehat{a}\rho_S(t)\widehat{a}^\dagger + \rho_S(t)\widehat{a}^\dagger \widehat{a}] &\end{aligned} \tag{4.14}$$

where

$$\bar{n}_{th} = \bar{n}_{k_0}(k = \omega/c) \tag{4.15}$$

4.2 Damping in Ion Trap system

Now we discuss the damping happening in our system. We still consider the total Hamiltonian applying on trapped ion,

$$\widehat{H} = \widehat{H}_m + \widehat{H}_e + \widehat{H}_d \tag{4.16}$$

where $\widehat{H}_d$ is Hamiltonian of random electric field applying on the ion

$$\widehat{H}_d = \sum_k g_k \widehat{b}_k e^{i(k\widehat{x}-\nu_k t)} + H.c. \tag{4.17}$$

k represents the mode of electric field existing in the trap. Like what we do in deriving Raman transition, we transform into interaction picture:

$$\begin{aligned}\widehat{H}_D &= \widehat{U}_0^\dagger \widehat{H}_d \widehat{U}_0 \\ &= \exp\left[\frac{i}{\hbar}(\widehat{H}_m + \widehat{H}_e)\right]\left[\sum_k g_k \widehat{b}_k e^{i(k\widehat{x}-\nu_k t)} + H.c.\right]\exp\left[-\frac{i}{\hbar}(\widehat{H}_m + \widehat{H}_e)\right]\end{aligned} \tag{4.18}$$

It is obvious that $[\widehat{H}_e, \widehat{H}_d] = 0$ because of $[\widehat{\sigma}_z, \widehat{b}_k/\widehat{b}_k^\dagger] = [\widehat{\sigma}_z, \widehat{x}] = 0$. So the term of exponent including $\widehat{H}_e$ vanishes. The left term of the interacting Hamiltonian becomes (For convenience we just discuss one mode) :

$$\widehat{H}_{D,k} = g_k \widehat{b}_k e^{-i\nu_k t} e^{-i\widehat{H}_m/\hbar} e^{ik\widehat{x}} e^{i\widehat{H}_m/\hbar} + g_k^* \widehat{b}_k^\dagger e^{-i\nu_k t} e^{-i\widehat{H}_m/\hbar} e^{-ik\widehat{x}} e^{i\widehat{H}_m/\hbar} \tag{4.19}$$

Inserting (3.6) into (4.19) with low orders expanding, we obtain the final form of the Hamiltonian:

$$\begin{aligned}\widehat{H}_{D,k} &= g_k \widehat{b}_k e^{-i\nu_k t} + g_k^* \widehat{b}_k^\dagger e^{i\nu_k t} \\ &+ i\eta g_k \widehat{a}^\dagger \widehat{b}_k e^{i(\nu-\nu_k)t} - i\eta g_k^* \widehat{a}\widehat{b}_k^\dagger e^{-i(\nu-\nu_k)t} \\ &+ i\eta g_k \widehat{a}\widehat{b}_k e^{-i(\nu+\nu_k)t} - i\eta g_k^* \widehat{a}^\dagger \widehat{b}_k^\dagger e^{i(\nu+\nu_k)t}\end{aligned} \tag{4.20}$$

The first two terms are nothing with interaction so they can be rescaled. The last term can be neglected because of rotating-wave approximation. The final form of interacting Hamiltonian is:

$$\widehat{H}_D = \sum_k \widehat{H}_{D,k} = \sum_k [G_k \widehat{a}^\dagger \widehat{b}_k e^{i(\nu-\nu_k)t} + G_k^* \widehat{a}\widehat{b}_k^\dagger e^{-i(\nu-\nu_k)t}] \tag{4.21}$$

on substituting $G_k = i\eta g_k$

Now comparing (4.21) with (4.7), we find that these two Hamiltonian are the same. Considering it is thermal equilibrium in trap space, we assume that the modes of random electric fluctuation are also thermal equilibrium. So we can directly obtain that without other driven Hamiltonian, the density matrix will evolve in

the way described in (4.14). If we take other driven Hamiltonian, just like Raman transition, into account, the Master equation is like:

$$\begin{aligned}\dot{\rho} &= -\frac{i}{\hbar}[\rho, \widehat{H}_I] \\ &- \bar{n}_{th}\frac{\Gamma}{2}[\widehat{a}\widehat{a}^\dagger\rho - 2\widehat{a}^\dagger\rho\widehat{a} + \rho\widehat{a}\widehat{a}^\dagger] - (\bar{n}_{th}+1)\frac{\Gamma}{2}[\widehat{a}^\dagger\widehat{a}\rho - 2\widehat{a}\rho\widehat{a}^\dagger + \rho\widehat{a}^\dagger\widehat{a}]\end{aligned} \tag{4.22}$$

4.3 Solution to Quantum Damping

Based on the Master equation (4.22), we analysis pure damping process at first (with $\widehat{H}_I = 0$). The evolution equation we have got is:

$$\dot{\rho} = -\frac{\Gamma}{2}\bar{n}_{th}[\widehat{a}\widehat{a}^\dagger\rho - 2\widehat{a}^\dagger\rho\widehat{a} + \rho\widehat{a}\widehat{a}^\dagger] - \frac{\Gamma}{2}(1+\bar{n}_{th})[\widehat{a}^\dagger\widehat{a}\rho - \widehat{a}\rho\widehat{a}^\dagger + \rho\widehat{a}^\dagger\widehat{a}] \tag{4.23}$$

In fact it is hard to get exact solution of this equation. Instead of solving this equation directly, we transform it into P-representation, which is one of the most important representation in quantum optics. In P-representation, a density matrix can be represented as:

$$\rho = \int P(\alpha, \alpha^*)|\alpha\rangle\langle\alpha|\mathrm{d}^2\alpha \tag{4.24}$$

Inserting (4.24) into (4.23), we have

$$\begin{aligned}&\int \dot{P}(\alpha,\alpha^*,t)|\alpha\rangle\langle\alpha|\mathrm{d}^2\alpha \\ &= -\frac{\Gamma}{2}\bar{n}_{th}\int P(\alpha,\alpha^*,t)(\widehat{a}\widehat{a}^\dagger|\alpha\rangle\langle\alpha| - 2\widehat{a}^\dagger|\alpha\rangle\langle\alpha|\widehat{a} + |\alpha\rangle\langle\alpha|\widehat{a}\widehat{a}^\dagger)\mathrm{d}^2\alpha \\ &- \frac{\Gamma}{2}(1+\bar{n}_{th})\int P(\alpha,\alpha^*,t)(\widehat{a}^\dagger\widehat{a}|\alpha\rangle\langle\alpha| - 2\widehat{a}|\alpha\rangle\langle\alpha|\widehat{a}^\dagger + |\alpha\rangle\langle\alpha|\widehat{a}^\dagger\widehat{a})\mathrm{d}^2\alpha\end{aligned} \tag{4.25}$$

After substituting the relations below,

$$\begin{aligned}
&\widehat{a}|\alpha\rangle\langle\alpha| = \alpha|\alpha\rangle\langle\alpha| \\
&\widehat{a}^{\dagger}|\alpha\rangle\langle\alpha| = (\frac{\partial}{\partial\alpha} + \alpha^*)|\alpha\rangle\langle\alpha| \\
&|\alpha\rangle\langle\alpha|\widehat{a}^{\dagger} = \alpha^*|\alpha\rangle\langle\alpha| \\
&|\alpha\rangle\langle\alpha|\widehat{a} = (\frac{\partial}{\partial\alpha^*} + \alpha)|\alpha\rangle\langle\alpha|
\end{aligned} \tag{4.26}$$

we simplify the equation and obtain:

$$\begin{aligned}
&\int \dot{P}(\alpha,\alpha^*,t)|\alpha\rangle\langle\alpha|\mathrm{d}^2\alpha = \\
&\int \frac{\Gamma}{2}P(\alpha,\alpha^*,t)(-\alpha\frac{\partial}{\partial\alpha} - \alpha^*\frac{\partial}{\partial\alpha^*} + 2\bar{n}_{th}\frac{\partial^2}{\partial\alpha\partial\alpha^*})|\alpha\rangle\langle\alpha|\mathrm{d}^2\alpha
\end{aligned} \tag{4.27}$$

Through integration by parts, we can simplify it further more

$$\begin{aligned}
&\int \dot{P}(\alpha,\alpha^*,t)|\alpha\rangle\langle\alpha|\mathrm{d}^2\alpha = \\
&\int \frac{\Gamma}{2}(\frac{\partial}{\partial\alpha}\alpha + \frac{\partial}{\partial\alpha^*}\alpha^* + 2\bar{n}_{th}\frac{\partial^2}{\partial\alpha\partial\alpha^*})P(\alpha,\alpha^*,t)|\alpha\rangle\langle\alpha|\mathrm{d}^2\alpha
\end{aligned} \tag{4.28}$$

For the establishing of (4.28), the integrated parts should be same, which means:

$$\dot{P} = \frac{\Gamma}{2}(\frac{\partial}{\partial\alpha}\alpha + \frac{\partial}{\partial\alpha^*}\alpha^* + 2\bar{n}_{th}\frac{\partial^2}{\partial\alpha\partial\alpha^*})P \tag{4.29}$$

Now it is still hard to solve the equation (4.29). In order to understand the result of quantum damping, we want to know how the state becomes after enough time for damping. The steady solution can satisfy our needs. Assuming $\dot{P} = 0$, we have steady equation:

$$\frac{\Gamma}{2}(\frac{\partial}{\partial\alpha}\alpha + \frac{\partial}{\partial\alpha^*}\alpha^* + 2\bar{n}_{th}\frac{\partial^2}{\partial\alpha\partial\alpha^*})P = 0 \tag{4.30}$$

Considering the solution in Gaussian form:

$$P_g(\alpha,\alpha^*)=\frac{1}{\pi\mu}\exp\left(-\frac{|\alpha-\alpha_0|^2}{\mu}\right) \tag{4.31}$$

Inserting (4.31) into (4.30), we get

$$(1-\frac{\bar{n}_{th}}{\mu})+\frac{\bar{n}_{th}(|\alpha|^2+|\alpha_0|^2)-\mu|\alpha|^2}{2\mu^2}+\frac{(\alpha\alpha_0^*+\alpha^*\alpha_0)(2\bar{n_{th}}-\mu)}{2\mu^2}=0 \tag{4.32}$$

It should be established for any α value. The only satisfied solution is

$$\mu=\bar{n}_{th}\qquad \alpha_0=0 \tag{4.33}$$

So the final steady solution is

$$P_{steady}(\alpha,\alpha^*)=\frac{1}{\pi\bar{n}_{th}}\exp\left(-\frac{|\alpha|^2}{\bar{n}_{th}}\right) \tag{4.34}$$

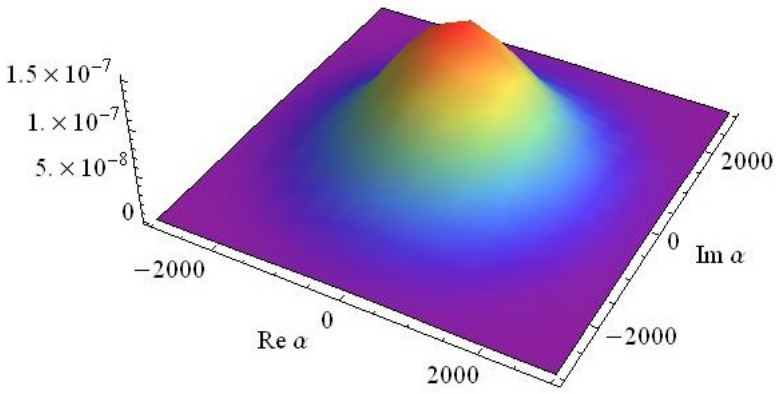

Figure 4.2: Steady solution in P-representation.

Fortunately, (4.34) is the P-function of thermal state with average phonon number $\bar{n}_{th}$. Because the initial P-function is not specific, so this steady solution is applicative for any initial state. This point means that, whatever initial state is, after enough time for quantum damping (without any other driven Hamiltonian),

the state will develop into thermal state. Especially, for an initial thermal state, the state will keep in thermal with $\bar{n}_{th}$ increasing.

Now we discuss about increasing of average phonon number in quantum damping process. As I mentioned before the average phonon number express as:

$$\langle n\rangle = \sum_i i p_i = \sum_i i\rho_{i,i} \tag{4.35}$$

It is obvious that $\rho_{i,i} = |c_i|^2 = p_i$ in Fock state basis. So at the same way we transform (4.23) into Fock state basis, by multiplying $\langle i|$ and $|i\rangle$ at right and left, the result is

$$\dot{p}_i = -\Gamma\bar{n}_{th}[(i+1)p_i - ip_{i-1}] - \Gamma(\bar{n}_{th}+1)[ip_i - (i+1)p_{i+1}] \tag{4.36}$$

We can derived the rate of average phonon changing over time:

$$\begin{aligned}\langle\dot{n}\rangle &= \sum_i i\dot{p}_i \\ &= \sum_i i[-\Gamma\bar{n}_{th}[(i+1)p_i - ip_{i-1}] - \Gamma(\bar{n}_{th}+1)[ip_i - (i+1)p_{i+1}]]\end{aligned} \tag{4.37}$$

After reforming, we can simplify (4.37) as

$$\begin{aligned}\langle\dot{n}\rangle &= -\sum_i [i(i+1)\Gamma\bar{n}_{th}p_i - (i+1)^2\Gamma(\bar{n}_{th}+1)p_i \\ &+ i^2\Gamma(\bar{n}_{th}+1)p_i - i(i-1)\Gamma(\bar{n}_{th}+1)p_i] \\ &= [\Gamma\bar{n}_{th} - \Gamma(\bar{n}_{th}+1)]\sum_i i p_i + \Gamma\bar{n}_{th}\sum_i p_i \\ &= -\Gamma\langle n\rangle + \Gamma\bar{n}_{th}\end{aligned} \tag{4.38}$$

(4.38) can be easily solved, the common solution is

$$\langle n(t)\rangle = \bar{n}_{th} - (\bar{n}_{th} - \bar{n}_0)e^{-\Gamma t} \tag{4.39}$$

where $\bar{n}_0 = \langle n(0) \rangle$ is given as boundary condition.

Assuming Γt is small enough, so (4.39) can be approximated as

$$\langle n(t) \rangle \approx \bar{n}_0 + \Gamma(\bar{n}_{th} - \bar{n}_0)t \tag{4.40}$$

$\langle \dot{n}(t) \rangle = \Gamma(\bar{n}_{th} - \bar{n}_0)$ is called as heating rate. Especially, when $\bar{n}_{th} \gg \bar{n}_0$, the heating rate is approximately equal to $\Gamma \bar{n}_{th}$

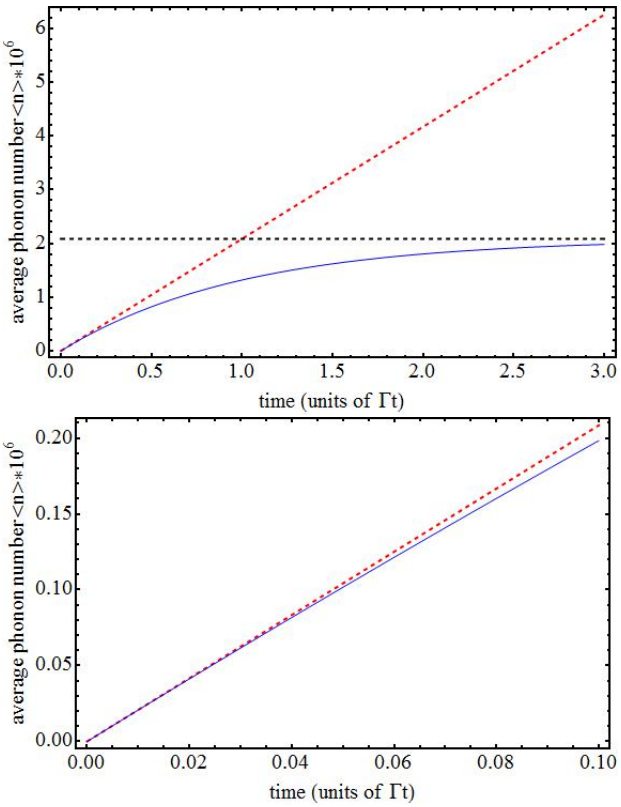

Figure 4.3: The increasing of average phonon number. The upper one shows the long time process of phonon increase. The blue solid line shows the phonon increasing with time and will reach the phonon number of the reservoir (black dashed line) for infinity time. The lower one shows the linear approximation of increasing is proper in short time process (red dashed line). But deviation is obvious for long time process (shown in upper one).

That means, for Γt is small enough, the average phonon number increase linearly at the speed of $\Gamma \bar{n}_{th}$. So does the temperate increase linearly too. It is easy to

understand why researchers regard quantum damping as a heating effect in the ion trap system. Moreover, because the off-diagonal terms of density matrix of thermal state are all zero, so the quantum damping will also destroy the coherence between phonon state of the initial state.

Finally, considering there are still other heating effects in the system just like collision with gas molecule, the actual value of Γ_{eff} is larger than what we get above.

4.4 Experiments in Ion Trap System

4.4.1 State Preparation

After Optical pumping, Doppler cooling and resolved sideband cooling, the final state of ion is $|0\rangle$. Then with series π pulse of blue sideband transition and carrier sideband transition, ideally we can get any $|n\rangle$ we want.

Considering several effects will affect our process, just like imperfect sideband transition (make error both in sideband cooling and high n state preparation) and damping process, so the prepared states are not perfect in state we want. We define infidelity as $1-\sqrt{p_n}$, where p_n is the population in the Fock state. In this experiment the value of n is up to 5. The infidelities of the prepared Fock states are showed in Table 4.1

Table 4.1: Infidelities of Fock State Preparation

n	**0**	**1**	**2**	**3**	**4**	**5**
Measured infidelity(%)	2.3	2.8	5.2	3.9	7.8	10.4
Simulated infidelity(%)	1.4	1.7	2.5	2.9	5.7	8.7

4.4.2 Phonon Reconstruction

After state preparation, we wait certain time (from hundreds of microseconds to thousands of microseconds) for quantum damping process. After that, we drive

blue sideband transition and detect its Rabi oscillation. The next problem is that how we can reconstruct the phonon distribution through the result of Rabi oscillation. According to (3.13), the Rabi oscillation is composed of several independent oscillation with certain Rabi frequency $\Omega_{n,n+1}$. So the Fourier transformation is a choice to realize the phonon reconstruction. However because of damping process, there are some corrections to (3.13). The experimental results of Rabi oscillation are in the form of:

$$P_{\uparrow,bsb}(t) = \sum_{n=0}^{\infty} \frac{1}{2} p_n [1 - e^{-\gamma_n t} \cos(\Omega_{n,n+1} t)] \tag{4.41}$$

So we can use fitting method to reconstruct phonon distribution[27], the fitting equation is:

$$\chi^2 = \frac{1}{N} \sum_{n=0}^{n=n_{max}} (P_{\uparrow,bsb}(p_n, \gamma_n, \Omega_{n,n+1}) - P_{measure})^2 \tag{4.42}$$

Where N is the number of points on the blue transition curve. The aim of fitting is to find the minimum of (4.42). the n_{max} is the cutting for the fitting when there is almost no distribution in high phonon number. And we assume $\gamma_n = \gamma$ for any quantum number n.

However another problem of fitting is $\Omega_{n,n+1}$. One way is that we choose the approximate form $\Omega_{n,n+1} = \eta\Omega\sqrt{n+1}$. Another way is to use exact form:

$$\Omega_{n,n+1} = \Omega_0 e^{-\eta^2/2} \eta \sqrt{\frac{1}{n+1}} L_n^1(\eta^2) \tag{4.43}$$

Obviously the second way is more precise. In order to determine the value of η, we prepare enough Fock state from $|n = 0\rangle$ to $|n = 20\rangle$ then detect Rabi oscillation to get the value of Rabi frequency of each motional state. We fit the data by the equation of (4.43) and find the $\eta \approx 0.098$.

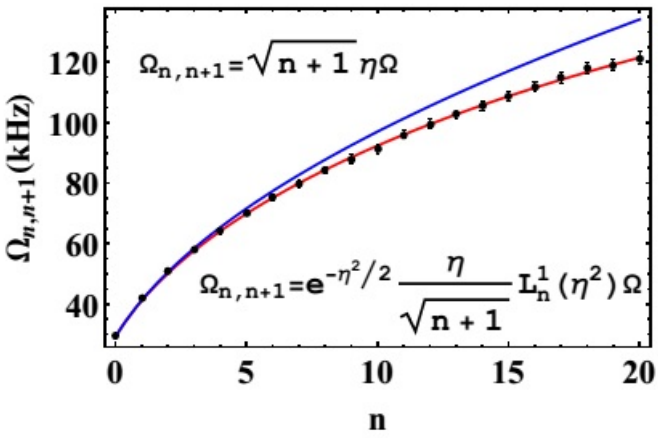

Figure 4.4: $\Omega_{n,n+1}$ for different n. The red line is obtained by fitting the measured blue sideband Rabi frequency (dots) with the exact formula and the blue line comes from the approximate expression of $\sqrt{n+1}$

Finally, the fitting parameters include p_n, γ and Ω_0. The set of p_n making (4.42) minimum is the phonon distribution we want to obtain.

4.4.3 Experimental Results

Our steps to measure the damping progress are:

1. Preparing Fock state from $|n=0\rangle$ to $|n=5\rangle$.
2. Waiting certain time for quantum damping process (waiting time is equal to 0, 250, 500, 750, 1000, 1500, 2000, 3000, 4000, 5000, 6000, 7000 μs).
3. Applying blue sideband transition after certain time.
4. Reconstructing phonon distribution by analyzing the interference pattern from different frequencies of Rabi oscillation depending on motional quantum number.

First we measure the quantum damping process of $|0\rangle$, which as I mentioned before the state will keep in thermal over the whole damping process. So we obtain the Rabi oscillation of blue sideband transition at each certain time, then reconstruct the phonon distribution of each time. Additionally, for thermal state, the phonon

distribution is

$$p_n = (\bar{n}_{th})^n/(\bar{n}_{th}+1)^{n+1} \tag{4.44}$$

where $\bar{n}_{th}$ is average phonon number and n is quantum number of motional state. Finally we fit the phonon distribution again by the form (4.44) then get the average phonon number of each time. The results of Rabi oscillation and reconstruction of phonon distribution are shown below:

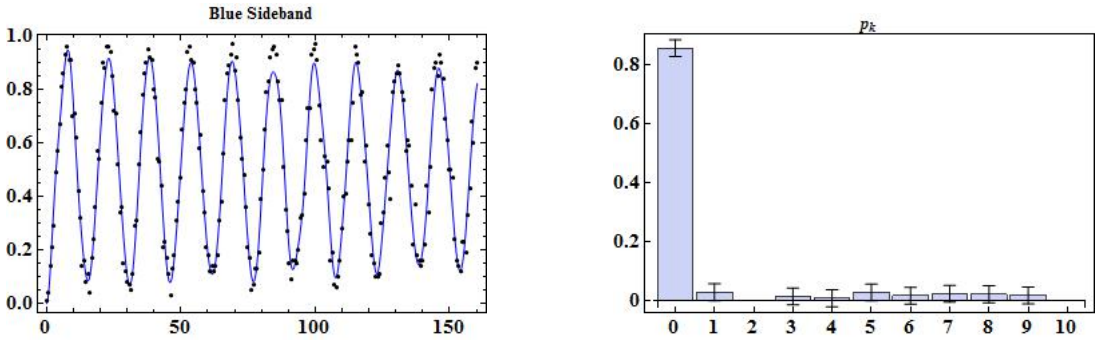

(a) t=0 μs

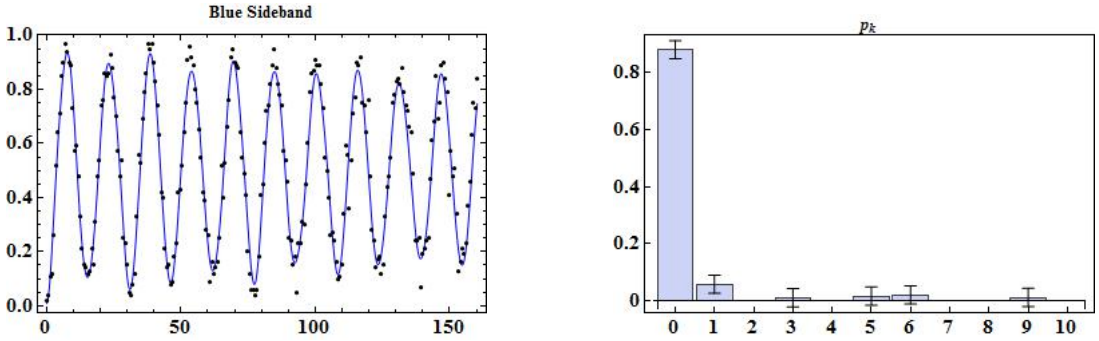

(b) t=250 μs

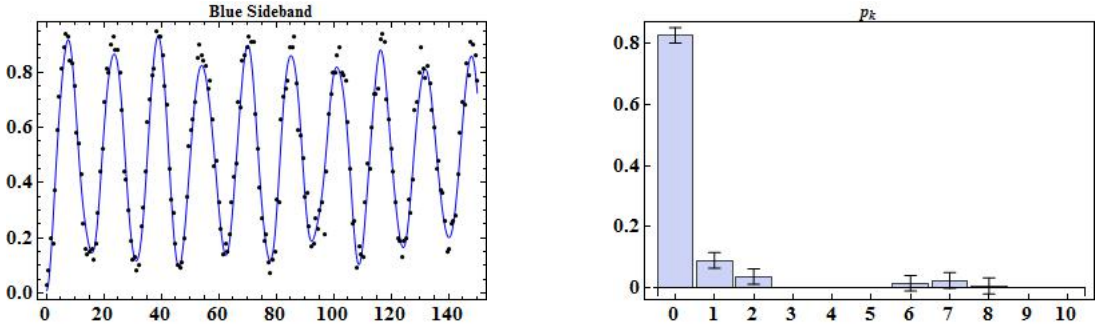

(c) t=500 μs

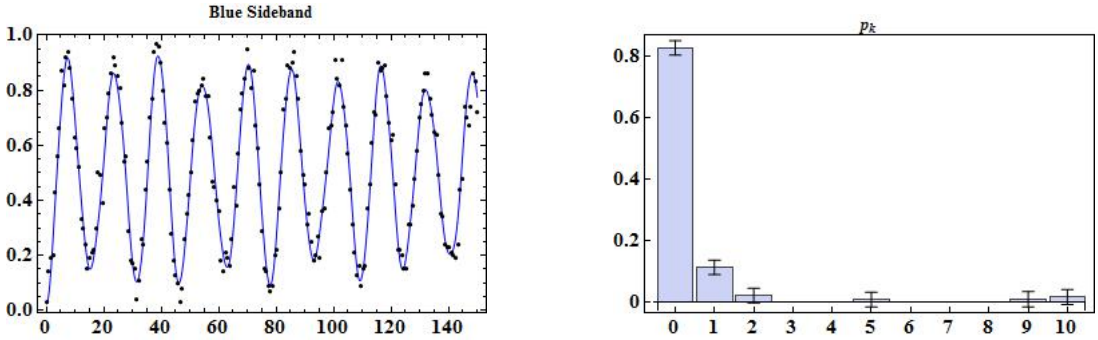

(d) t=750 μs

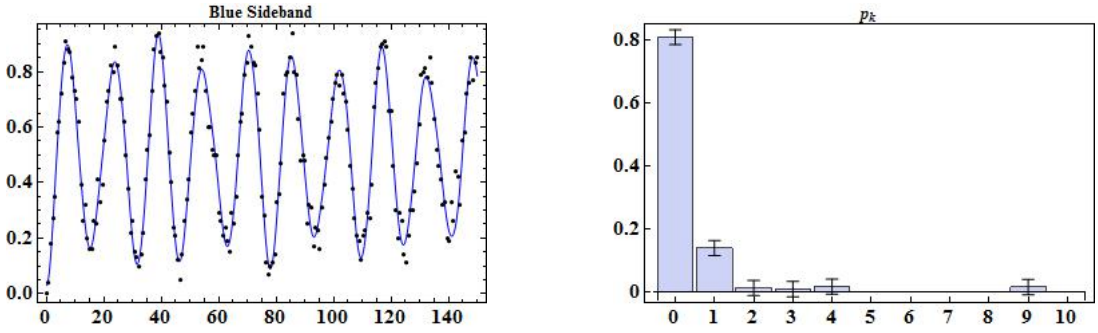

(e) t=1000 μs

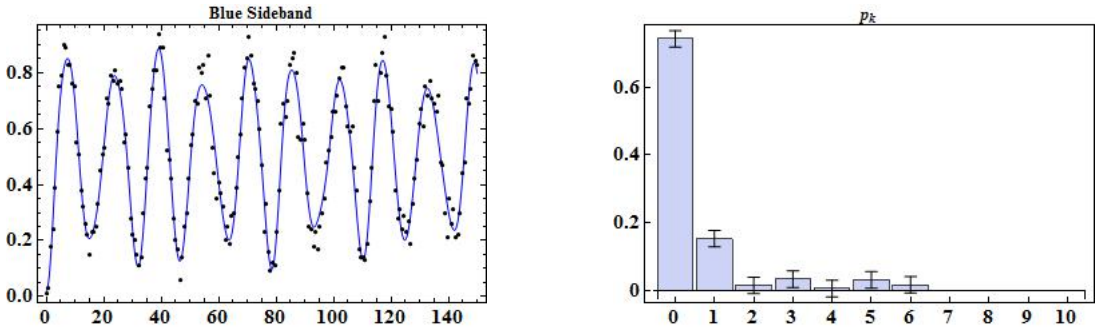

(f) t=1500 μs

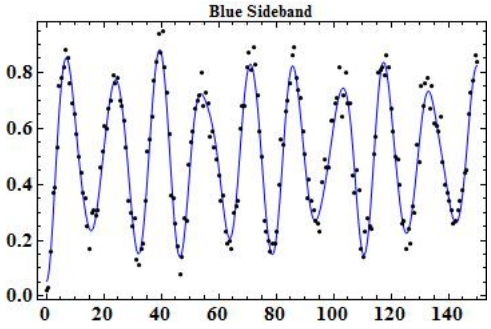

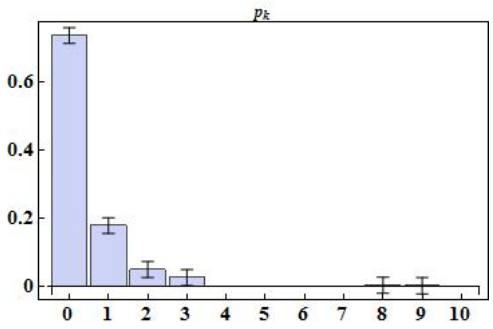

(g) t=2000 μs

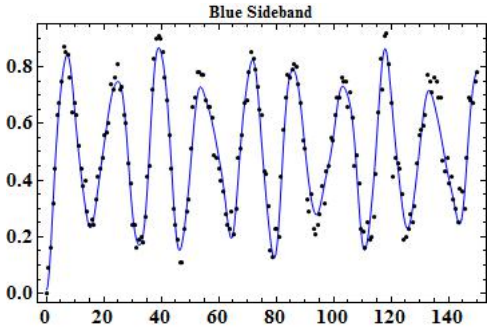

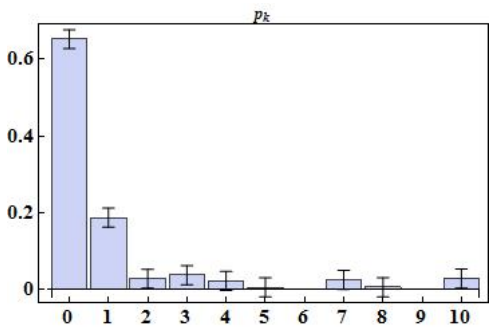

(h) t=2500 μs

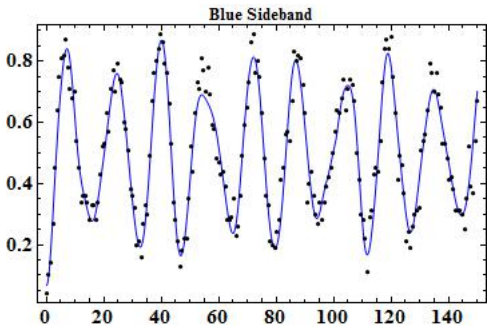

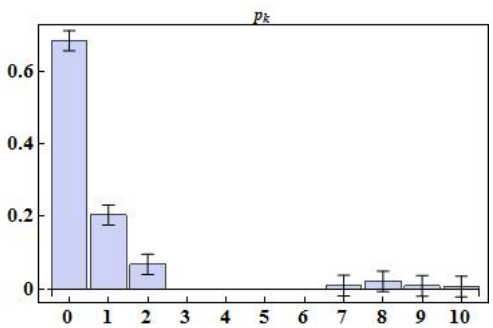

(i) t=3000 μs

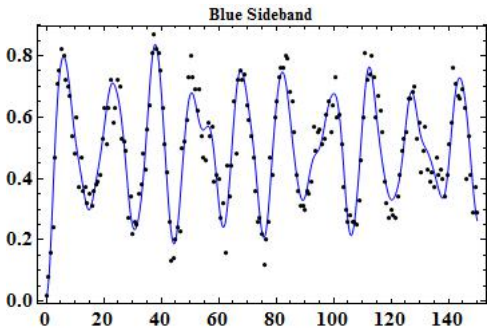

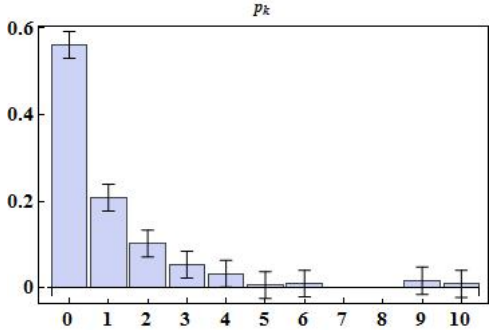

(j) t=4000 μs

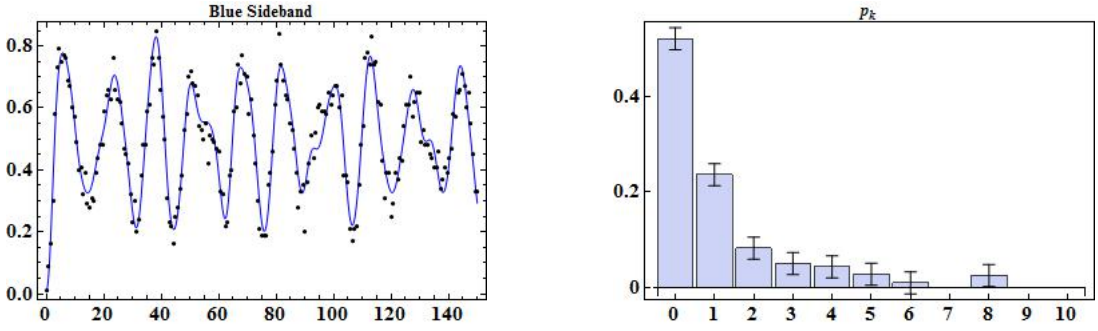

(k) t=5000 μs

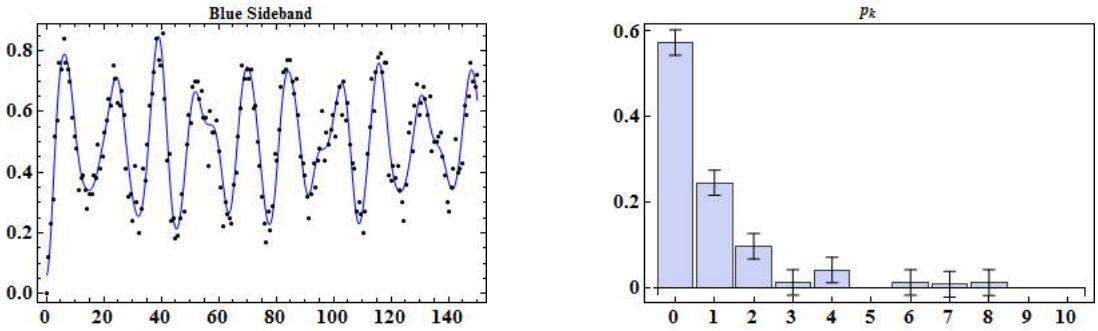

(l) t=6000 μs

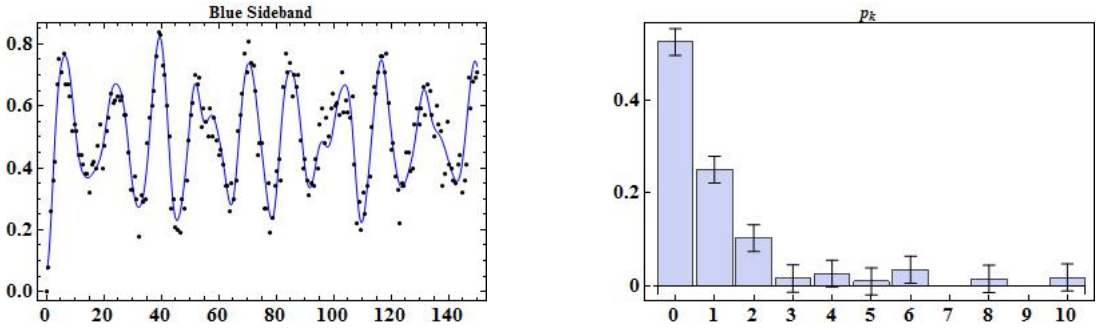

(m) t=7000 μs

Figure 4.5: Quantum damping process of initial thermal state $|0\rangle$.

To fit the phonon distribution of each time, we get the average phonon number at certain time:

Table 4.2: Average phonon number in quantum damping

time (μs)	$\langle n \rangle$
0	0.103 ± 0.059
250	0.106 ± 0.033
500	0.179 ± 0.045
750	0.188 ± 0.026
1000	0.223 ± 0.026
1500	0.311 ± 0.063
2000	0.352 ± 0.023
2500	0.483 ± 0.100
3000	0.445 ± 0.045
4000	0.771 ± 0.090
5000	0.903 ± 0.122
6000	0.727 ± 0.083
7000	0.870 ± 0.126

According to Table 4.2, heating rate can be obtained if we fit the data in the form of (4.40), with $\bar{n}_{th} - \bar{n}_0 \approx \bar{n}_{th}$:

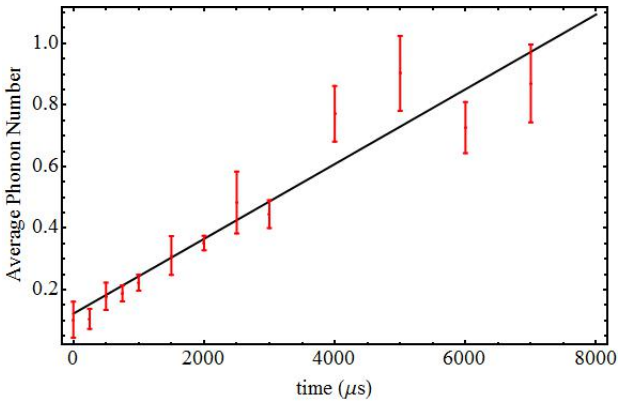

Figure 4.6: Average phonon number increases over time with initial state $|0\rangle$. The increasing can be nearly regarded as linear increasing.

According to the fitting result, the heating rate $\Gamma\bar{n}_{th}$ is approximately equal to 121 Hz. Actually damping process of $|1\rangle$ to $|5\rangle$ also has been done. In order to understand process of quantum damping more intuitively, we also simulate the process of quantum damping in Mathematica. To compare the results between simulation and experiment, we plot them together:

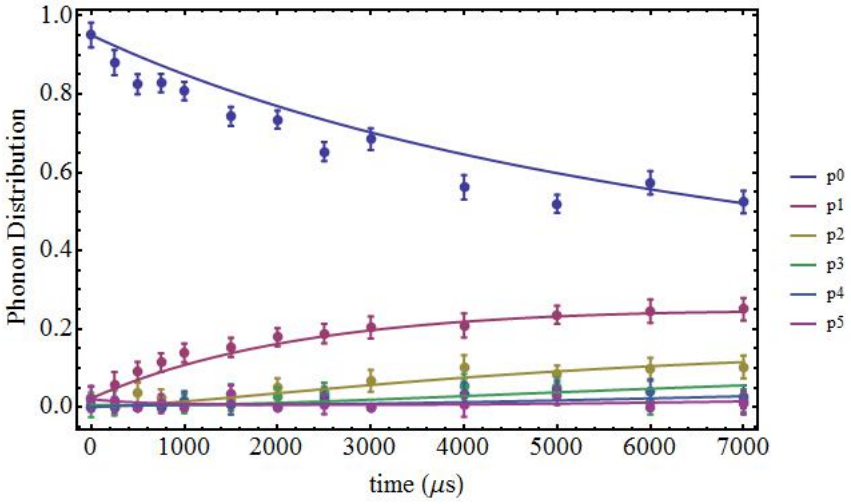

(a) Initial state $|0\rangle$

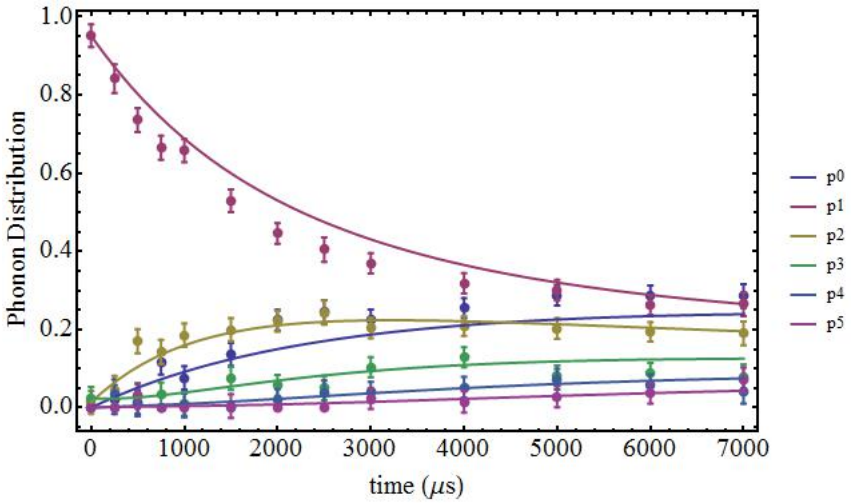

(b) Initial state $|1\rangle$

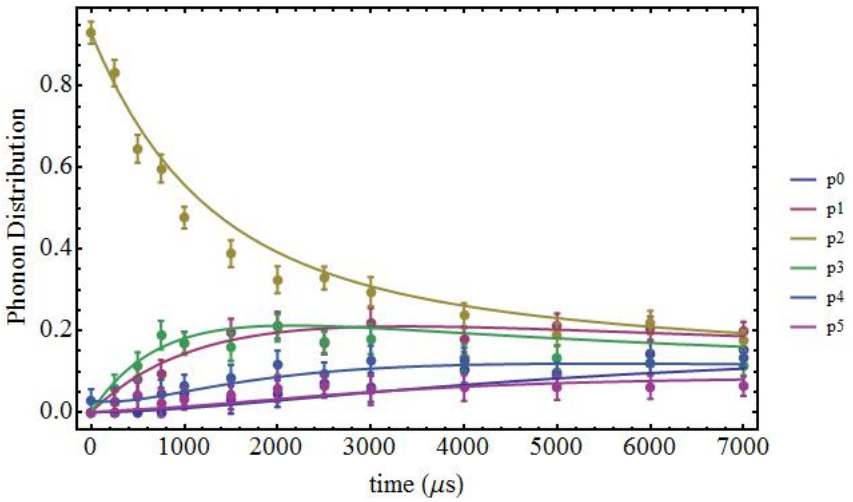

(c) Initial state $|2\rangle$

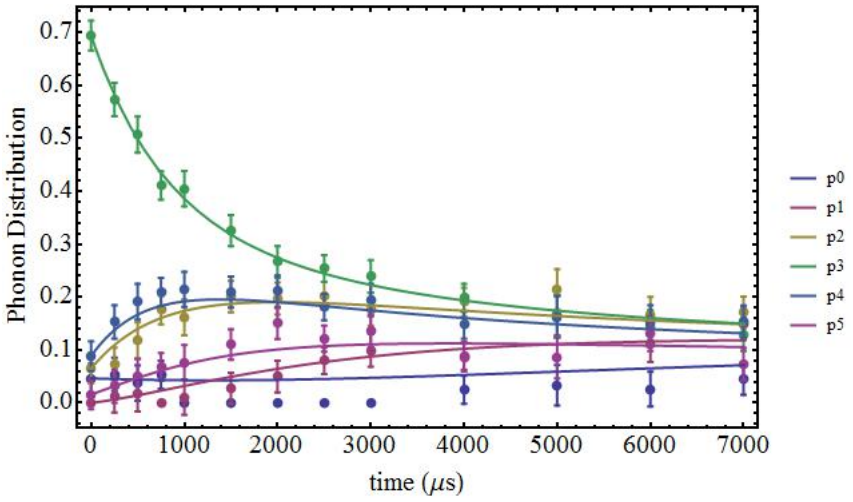

(d) Initial state $|3\rangle$

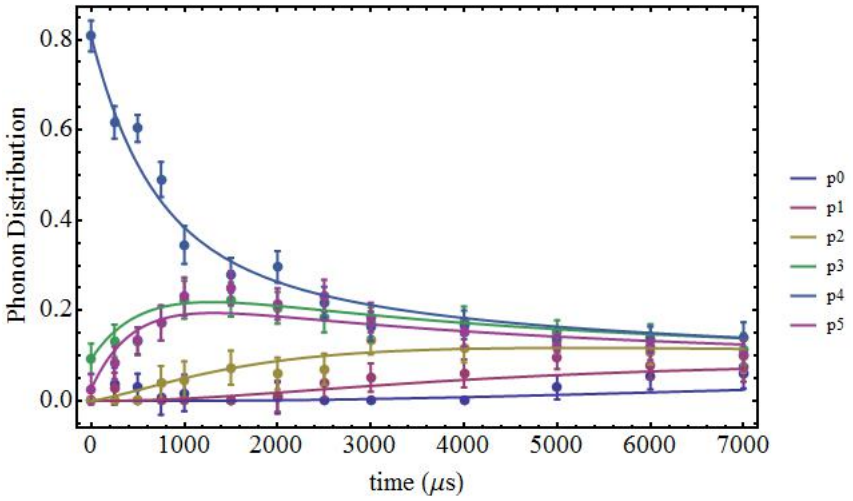

(e) Initial state $|4\rangle$

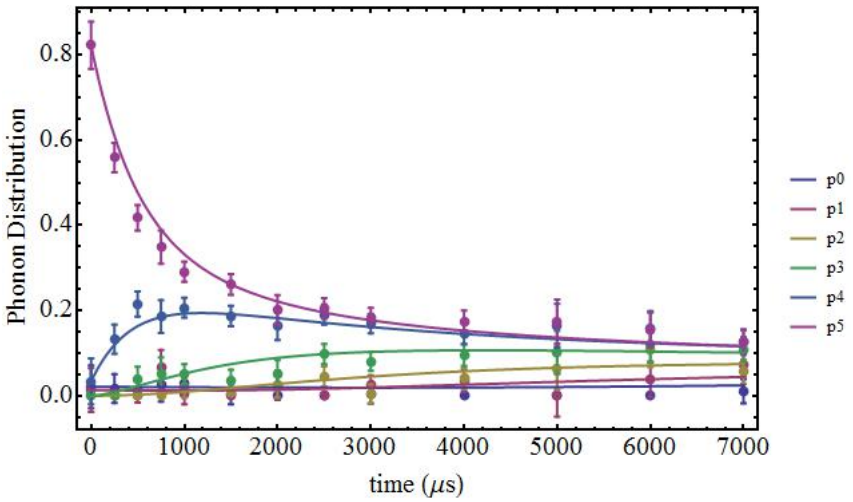

(f) Initial state $|5\rangle$

Figure 4.7: Evolution of phonon distribution by quantum distribution. (a) to (f) represents initial state from $|0\rangle$ to $|5\rangle$ separately.

It is obviously to see that the results of simulation and experiment are consistent. We also notice that, with increasing of the quantum number of initial state, the damping speed also increase. According to (4.36), we find that the rate from $|n\rangle$ to $|n-1\rangle$ and from $|n\rangle$ to $|n+1\rangle$ is proportional to $\sqrt{n}$ and $\sqrt{n+1}$, which is the result of $\widehat{a}$ and $\widehat{a}^{\dagger}$. Thus for the state of high quantum number, the spreading of distribution is more fast.

Chapter 5

Conclusion

The quantum damping is just the simplified model of motional decoherence and heating effect in ion trap system. Although the decoherence caused by quantum damping will destroy the phase relationship between motional state, reduce the efficiency of quantum detection. Sometimes it is helpful when we want to generate some special state. Take thermal state for example. As I mentioned before, the state will keep in thermal if the initial state is thermal state. For the state after ideal optical pumping, ion is located at $|0\rangle$ which is the simplest thermal state for $\bar{n} = 0$. So if we generate $|0\rangle$ at first, without other driving Hamiltonian, we can get any thermal state with any average phonon number theoretically.

For our recent research about quantum Jarzynski equality[28], an initial thermal state is required. If we apply a force on the ion, the work (W) done on the ion and the difference of the free energy ΔF between initial state and state after obtaining work have relationship below:

$$\langle e^{-(W-\Delta F)/k_B T} \rangle = 1 \tag{5.1}$$

Jarzynski equality is the generalization of Clausius inequality. The former can be applied to any situation even far-away from equilibrium, while the latter is only suitable for equilibrium for $W = \Delta F$.

Additionally, on the one hand, we will do further research on Crooks fluctuation

theorem[29], which thermal state is still required. On the other hand, lowering the heating rate is also required for more precise experiment, for example the projective measurement and the construction of Wigner function[30].

References

[1] R. P. Feynman. "*Simulating physics with computers*". *International Journal of Theoretical Physics*, **1982**, *21*(6): 467–488.

[2] R. Hughes and J. Nordholt. "*Refining quantum cryptography*". *Science*, **2011**, *333*(6049): 1584–1586.

[3] L. L. Sohn, L. P. Kouwenhoven, *et al. Mesoscopic Electron Transport: Proceedings of the NATO Advanced Study Institute*. Springer, **1997**.

[4] Y. Nakamura, Y. A. Pashkin and J. Tsai. "*Coherent control of macroscopic quantum states in a single-Cooper-pair box*". *Nature*, **1999**, *398*(6730): 786–788.

[5] B. E. Kane. "*A silicon-based nuclear spin quantum computer*". *Nature*, **1998**, *393*(6681): 133–137.

[6] J. I. Cirac, P. Zoller, *et al.* "*Quantum computations with cold trapped ions*". *Physical Review Letters*, **1995**, *74*(20): 4091–4094.

[7] J. L. O'Brien. "*Optical quantum computing*". *Science*, **2007**, *318*(5856): 1567–1570.

[8] N. A. Gershenfeld and I. L. Chuang. "*Bulk spin-resonance quantum computation*". *Science*, **1997**, *275*(5298): 350–356.

[9] D. Wineland, P. Ekstrom and H. Dehmelt. "*Monoelectron oscillator*". *Physical Review Letters*, **1973**, *31*(21): 1279–1282.

[10] W. Paul. "*Electromagnetic traps for charged and neutral particles*". **1990**.

[11] A. Shuoming. "*Frequency Comb Application for The Coherent Control of Trapped Ions*". Bachelor thesis, **2012**, Peking University.

[12] D. Wineland *et al.* "*Experimental issues in coherent quantum-state manipulation of trapped atomic ions*". *Journal of Research of the National Institute of Standards and Technology*, **1998**, *103*(3): 259–328.

[13] S. M. Olmschenk. "*Quantum teleportation between distant matter qubits*". Ph.D thesis, **2009**, University of Maryland.

[14] D. Leibfried *et al.* "*Quantum dynamics of single trapped ions*". *Reviews of Modern Physics*, **2003**, *75*(1): 281.

[15] A. Chew. "*Doppler-free spectroscopy of iodine at 739nm*". Ph.D thesis, **2008**, The University of Michigan.

[16] Z. Junhua. "*Developing a Control System for Quantum Information Processing with Trapped Ions*". Bachelor thesis, **2012**, Peking University.

[17] F. Diedrich *et al.* "*Laser cooling to the zero-point energy of motion*". *Physical Review Letters*, **1989**, *62*(4): 403–406.

[18] C. Foot. *Atomic Physics*. Oxford University Press, **2008**.

[19] T. R. Carver. "*Optical pumping*". *Science*, **1963**, *141*(3581): 599–608.

[20] S. Olmschenk *et al.* "*Manipulation and detection of a trapped Yb^+ hyperfine qubit*". *Physical Review. A*, **2007**, *76*(5).

[21] C. Monroe *et al.* "*Resolved-sideband Raman cooling of a bound atom to the 3D zero-point energy*". *Physical Review Letters*, **1995**, *75*(22): 4011.

[22] Q. Turchette *et al.* "*Heating of trapped ions from the quantum ground state*". *Physical Review A*, **2000**, *61*(6): 063418.

[23] R. Epstein *et al.* "*Simplified motional heating rate measurements of trapped ions*". *Physical Review A*, **2007**, *76*(3): 033411.

[24] Q. Turchette *et al.* "*Decoherence and decay of motional quantum states of a trapped atom coupled to engineered reservoirs*". *Physical Review A*, **2000**, *62*(5): 053807.

[25] M. O. Scully. *Quantum Optics*. Cambridge University Press, **1997**.

[26] F. Intravaia *et al.* "*Quantum theory of heating of a single trapped ion*". *Physics Letters A*, **2003**, *308*(1): 6–10.

[27] U. Poschinger. *Quantum Optics Experiments in a Microstructured Ion Trap*, **2010**.

[28] C. Jarzynski. "*Nonequilibrium equality for free energy differences*". *Physical Review Letters*, **1997**, *78*: 2690.

[29] G. E. Crooks. "*Entropy production fluctuation theorem and the nonequilibrium work relation for free energy differences*". *Physical Review E*, **1999**, *60*(3): 2721.

[30] D. Leibfried *et al.* "*Experimental determination of the motional quantum state of a trapped atom*". *Physical Review Letters*, **1996**, *77*(21): 4281.